A Hybrid Asymptotic-Numerical Method for Low Reynolds Number Flows Past Symmetric Cylindrical Bodies

M. C. A. Kropinski *

Courant Institute of Mathematical Sciences

New York University

New York, New York, 10012

Michael J. Ward †

Dept. of Mathematics

Univ. of British Columbia

Vancouver, British Columbia, V6T 1Y4

Joseph B. Keller ‡

Depts. of Mathematics and Mechanical Engineering

Stanford University

Stanford, Ca. 94305

Abstract

The classical problem of slow, steady, two-dimensional flow of a viscous incompressible fluid around an infinitely long straight cylinder is considered. The cylinder cross-section is symmetric about the direction of the oncoming stream, but otherwise is arbitrary. For low Reynolds number, the well-known singular perturbation analysis for this problem shows that the asymptotic expansions of the drag coefficient and of the flow field start with infinite logarithmic series. We show that the entire infinite logarithmic expansions of the flow field and of the drag coefficient are contained in the solution to a certain related problem that does not involve the cross-sectional shape of the cylinder. The solution to this related problem is computed numerically using a straightforward finite-difference scheme. The drag coefficient for a cylinder of a specific cross-sectional shape, which is asymptotically correct to within all logarithmic terms, is given in terms of a single shape-dependent constant that is determined by the solution to a canonical Stokes flow problem. The resulting hybrid asymptotic-numerical method is illustrated for cylinders of various cross-sectional shapes. For a circular cylinder, our results for the drag coefficient are compared with experimental results, with the explicit three-term asymptotic theory of Kaplun, and with numerical results computed from the full problem. A similar hybrid approach is used to sum infinite logarithmic expansions for a generalized version of Lagerstrom's ordinary differential equation model of slow viscous flow.

Key Words: logarithmic expansions, slow viscous flow, drag coefficient, finite differences.

* Supported by NSF grant DMS-9112654

† Supported by NSERC grant 5-81541

‡ Supported by the National Science Foundation, The Office of Naval Research and the Air Force Office of Scientific Research

1. Introduction

We consider the classical problem of slow, steady, two-dimensional flow of a viscous incompressible fluid around an infinitely long straight cylinder. The cross-sectional shape of the cylinder is assumed to be symmetric about the direction of the oncoming stream, but otherwise is arbitrary. By slow we mean that the Reynolds number $\epsilon = U_\infty L/\nu$ is small, where U_∞ is the velocity of the fluid at infinity, ν is the kinematic viscosity, and $2L$ is the diameter of the cross-section of the cylinder.

For $\epsilon \to 0$, the method of matched asymptotic expansions was used systematically by Kaplun [5] and by Proudman and Pearson [12] to resolve the well-known Stokes paradox, and to calculate asymptotically the stream function in both the Stokes region, which is near the body, and in the Oseen region, which is far from the body. These pioneering studies showed that, for $\epsilon \to 0$, the asymptotic expansion for the drag coefficient C_D of a circular cylindrical body starts with $C_D \sim 4\pi\epsilon^{-1}S(\epsilon)$, where $S(\epsilon)$ is an infinite series in powers of $1/\log\epsilon$. The coefficients in this series are determined in terms of the solutions to certain forced Oseen problems. For a cylinder of arbitrary cross-section, it was shown in [5] that $C_D \sim 4\pi\epsilon^{-1}S(\epsilon d)$, where d is an 'effective' radius of the cylinder. This result establishes a certain asymptotic equivalence for C_D between cylinders of various cross-sectional shapes and is known as Kaplun's equivalence principle. An infinite logarithmic series for the stream function in the Oseen region, which has the same equivalence property, was also obtained in [5].

In an effort to determine C_D quantitatively, analytical formulae for the first three coefficients in $S(\epsilon)$ were obtained in [5]. However, as a result of the slow decay of $1/\log\epsilon$ with decreasing values of ϵ, the resulting three-term truncated series for C_D agrees rather poorly with the experimental results of Tritton [16] unless ϵ is very small (cf. Van Dyke [18]). Because of the complexity of the calculations required, it is impractical to obtain a closer quantitative determination of the drag coefficient by calculating further coefficients in $S(\epsilon)$ analytically. As a result of these fundamental long-standing difficulties, the problem of slow viscous flow around a cylinder has served as a paradigm for problems where the method of matched asymptotic expansions fails to be of much practical use, unless ϵ is very small.

Recently, infinite logarithmic expansions have been found in problems unrelated to fluid mechanics. Such problems include the singularly perturbed linear and nonlinear eigenvalue problems that result from the removal of a small subdomain of radius ϵ from a two-dimensional domain (cf. [19] and [20]). For small ϵ, the asymptotic structure of the solutions to these eigenvalue problems is strikingly similar to that of the slow viscous flow problem. In particular, the expansion of the eigenvalue parameter for these problems starts with an infinite logarithmic series, and an analogue of Kaplun's equivalence principle is found to hold. In [19] (see also [20]) a hybrid asymptotic-numerical method requiring relatively simple numerical computations was used to sum these logarithmic series, and the results compared favorably with corresponding exact and numerical results over a rather large range of ϵ.

Our goal is to formulate and implement a related hybrid asymptotic-numerical method to sum the infinite logarithmic expansions that arise from the singular perturbation analysis of slow viscous flow around a

cylinder. This approach differs from the hybrid method employed in [9], in which numerical methods are used within the framework of the method of matched asymptotic expansions to calculate the first few coefficients in the logarithmic expansions of the flow field and the drag coefficient. Instead, we show that these entire infinite logarithmic series are contained in the solution to a certain related problem that does not involve the cross-sectional shape of the cylinder. This related problem is solved numerically in a straightforward way using a finite-difference scheme. To obtain the asymptotic drag coefficient for a cylinder of a specific cross-sectional shape, we need only compute *a single* shape-dependent constant, which is defined in terms of the solution to a canonical Stokes flow problem. In this sense, our method provides a numerical implementation of Kaplun's equivalence principle. For a circular cylinder, our hybrid results for the drag coefficient are compared with experimental results, with the three-term asymptotic theory, and with the numerical results for the full problem. The hybrid method is also used to calculate the asymptotic drag coefficient for cylinders of other cross-sectional shapes.

Our hybrid method does not incorporate the effect of the transcendentally small inertial terms arising from the Stokes region. Therefore, the upstream/downstream asymmetry in the flow field near the body, which becomes more prominent as the Reynolds number is increased, is not captured by our analysis. For a circular cylinder, the leading order effects of these inertial terms on the flow field and on the drag coefficient were analyzed in [14].

Before discussing the slow viscous flow problem, we illustrate our method on a generalized version of Lagerstrom's ordinary differential equation model of slow viscous flow (cf. [7]). In this simpler setting, where the key ideas are more easily introduced, the results obtained from the hybrid method are shown to agree rather well with the full numerical results.

The outline of this paper is as follows. In §2 we sum logarithmic expansions for a generalized version of Lagerstrom's model viscous flow problem. In §3 we formulate a hybrid asymptotic-numerical method for summing the infinite logarithmic expansions that arise from a singular perturbation analysis of slow viscous flow around a cylinder of arbitrary cross-section. The numerical methods used to solve the resulting hybrid problem and to solve the full problem for a circular cylinder are discussed in §4. Finally, in §5 we give some examples of the theory and we compare results for C_D obtained from the hybrid method with the corresponding experimental, asymptotic and full numerical results.

2. Logarithmic Expansions for a Generalization of Lagerstrom's Model Problem

First we consider the following generalization of Lagerstrom's model viscous flow problem:

$$u'' + \frac{1}{r}u' + f(u)u' = 0\,, \quad 0 < \epsilon \le r < \infty\,, \tag{2.1a}$$

$$\epsilon u' - \kappa u = 0\,, \quad \text{on} \;\; r = \epsilon\,, \tag{2.1b}$$

$$u \sim 1\,, \quad \text{as} \;\; r \to \infty\,. \tag{2.1c}$$

Here $\kappa > 0$ and $f(u)$ is an arbitrary smooth function satisfying $f(1) = 1$ and $f(u) > 0$ for $u > 0$. Lagerstrom's problem (cf. [7], [3] and the references therein), corresponds to the special case $f(u) = u$ and $\kappa = \infty$ in (2.1).

For $\epsilon \to 0$, the solution to (2.1) is readily constructed using singular perturbation techniques. In the outer region, where $r = O(1)$, u has an infinite logarithmic expansion of the form

$$u(r) = 1 + \sum_{j=1}^{\infty} \nu^j(z) u_j(r) + \cdots . \tag{2.2}$$

Here $\nu(z) \equiv -1/\log z$ and $z \equiv \epsilon d$, where $d > 0$ is a constant specified below. The justification of this form for the outer expansion is shown below upon matching to the inner solution. The u_j, for $j \geq 1$, satisfy equations of the form

$$Lu_j \equiv u_j^{''} + \left(\frac{1}{r} + 1\right) u_j^{'} = R_{j-1}\,, \quad 0 < r < \infty\,; \qquad u_j \to 0\,, \quad \text{as} \;\; r \to \infty\,, \tag{2.3}$$

where $R_0 = 0$ and $R_j \equiv R_j(u_1, .., u_j)$. The first two R_j are

$$R_1 = -f^{'}(1) u_1 u_1^{'}\,, \qquad R_2 = -f^{'}(1) \left(u_1 u_2\right)^{'} - \frac{1}{2} f^{''}(1) u_1^2 u_1^{'}\,. \tag{2.4}$$

The behavior of u_j as $r \to 0$ is determined below.

In the inner region, where $r = O(\epsilon)$, we define $\rho = \epsilon^{-1} r$ and $w(\rho) = u(\epsilon\rho)$. Then, by writing $w(\rho) = \sum_{j=1}^{\infty} \nu^j(z) w_j(\rho)$, we obtain from (2.1$a, b$) that $w_j(\rho) = a_j w_c(\rho)$, where a_j is an undetermined constant. Here w_c is the canonical inner solution, which satisfies

$$w_c^{''} + \frac{1}{\rho} w_c^{'} = 0\,, \quad 1 \leq \rho < \infty\,; \quad w_c^{'}(1) - \kappa w_c(1) = 0\,; \quad w_c \sim \log\left(\rho/d\right)\,, \quad \text{as} \;\; \rho \to \infty\,. \tag{2.5}$$

Clearly, $w_c(\rho) = \log\rho - \log[e^{-1/\kappa}]$ and $d = e^{-1/\kappa}$. In terms of r, the inner expansion is

$$u(r) = a_1 + \sum_{j=1}^{\infty} \nu^j(z) \left(a_j \log r + a_{j+1}\right) + \cdots . \tag{2.6}$$

By matching (2.6) to the outer expansion (2.2), we find that $a_1 = 1$ and that u_j, for $j \geq 1$, has the following singular behavior:

$$u_j(r) \sim a_j \log r + a_{j+1}\,, \quad \text{as} \;\; r \to 0\,. \tag{2.7}$$

For each $j \geq 1$, u_j satisfies (2.3) subject to (2.7). The constant a_{j+1}, which is independent of ϵ and of κ, is determined uniquely in terms of u_j. Thus, starting with $a_1 = 1$, the a_j for $j \geq 1$ are determined recursively from the infinite sequence of problems (2.3), (2.7).

For $\epsilon \to 0$, the 'flux' Q out of $r = \epsilon$ is given in terms of the a_j by

$$Q \equiv \epsilon \frac{du}{dr}\Big|_{r=\epsilon} = \nu(\epsilon d)\Big(\sum_{j=0}^{\infty} a_{j+1} \nu^j(\epsilon d) + \cdots\Big)\,, \tag{2.8}$$

where $\nu(\epsilon d) = -1/\log(\epsilon d)$ and $d = e^{-1/\kappa}$. Since, to within all logarithmic terms, Q *depends only on the product* ϵd, the form (2.8) displays an analogue of Kaplun's equivalence principle.

When $f(u) = u$, explicit formulae for a_2, a_3, and a_4 were given in [7]. (The formula for a_4 quoted in [7] is erroneous and was corrected in [3]). By extending the previous calculations to treat an arbitrary $f(u)$, we obtain

$$\begin{aligned} &a_2 = \gamma\,, \qquad a_3 = \gamma^2 - 2f^{'}(1)\log 2\,, \\ &a_4 = \frac{3}{2}f^{''}(1)I + [f^{'}(1)]^2\left(-6\log 2 + \frac{9}{2}\log 3 - \frac{3}{2}I\right) - 6\gamma f^{'}(1)\log 2 + \gamma^3\,. \end{aligned} \tag{2.9}$$

Here γ is Euler's constant and $I \approx 1.22856$. Thus, a four-term expansion for Q results from setting $a_1 = 1$ and using (2.9) in (2.8). Formulae for the first few outer terms u_j are given in Appendix A.

For Lagerstrom's problem, where $f(u) = u$ and $\kappa = \infty$, it was shown in [3] that the four-term expansion for Q agrees very poorly at moderate values of ϵ with the corresponding numerical results computed from the full problem (2.1). As is shown below, similar poor agreement is found for other choices of $f(u)$ and κ. To overcome this difficulty, we formulate and implement a hybrid asymptotic-numerical method for summing the infinite logarithmic expansions (2.2), (2.6) and (2.8). This new method was introduced in [19] and [20]. It will be used in §3-5 to treat the slow viscous flow problem.

We begin by letting $A^*(z)$ denote a function asymptotic to the terms written in the brackets on the right side of (2.8),

$$A^*(z) \sim \sum_{j=0}^{\infty} a_{j+1}\nu^j(z)\,. \tag{2.10}$$

Here $\nu(z)$ is any function for which $\nu(z) = -1/\log z + o[(\log z)^{-m}]$ for all $m > 0$ as $z \to 0$. In particular, we can choose $\nu(z) = -1/\log z$. In terms of $A^*(z)$, the inner expansion (2.6) is asymptotic to

$$u = A^*(z)\,[\nu(z)\log r - \nu(z)\log z] + \cdots\,. \tag{2.11}$$

The hybrid formulation to determine $A^*(z)$ is to solve (2.1a,c) for $r > 0$ subject to the singular behavior (2.11), which is to hold for $r \to 0$. Therefore, we obtain the following related problem for $A^*(z)$ and the auxiliary function $u_H \equiv u_H(r;z)$:

$$u_H^{''} + \frac{1}{r}u_H^{'} + f(u_H)u_H^{'} = 0\,, \quad 0 < r < \infty\,, \tag{2.12a}$$

$$u_H \to 1\,, \quad \text{as} \quad r \to \infty\,; \quad u_H = A^*(z)\nu(z)\,[\log r - \log z] + o(1)\,, \quad \text{as} \quad r \to 0\,. \tag{2.12b}$$

In terms of A^* and d, the asymptotic formula for the flux Q, valid to within all logarithmic terms, is

$$Q = Q^*(\epsilon d) + \cdots\,, \qquad Q^*(z) \equiv \nu(z)A^*(z)\,, \tag{2.13}$$

where $d = e^{-1/\kappa}$. Thus the hybrid formulation has replaced the infinite sequence of problems (2.3), (2.7) with the parameter-dependent problem (2.12). We anticipate that the asymptotic error estimate for (2.13) is $Q - Q^*(z) = O\,(z/\log z)$.

To solve (2.12) numerically, it is convenient to decompose u_H as

$$u_H(r;z) = 1 - Q^*(z)E_1(r) + u^*(r;z)\,, \qquad E_1(r) \equiv \int_r^{\infty} \eta^{-1}e^{-\eta}\,d\eta\,. \tag{2.14}$$

Then, using (2.14) and $E_1(r) = -\log r - \gamma + o(1)$ as $r \to 0$, we can write (2.12) as

$$Lu^* = \left(1 - f\left[1 - Q^* E_1(r) + u^*\right]\right)\left(Q^* r^{-1} e^{-r} + u^{*'}\right), \quad 0 < r < \infty, \tag{2.15a}$$

$$u^* \to 0, \quad \text{as} \quad r \to \infty, \tag{2.15b}$$

$$u^* = -Q^* \log z - 1 - Q^* \gamma + o(1), \quad \text{at} \quad r = 0, \tag{2.15c}$$

$$u^{*'} = Q^*, \quad \text{at} \quad r = 0. \tag{2.15d}$$

Here L is defined in (2.3). The conditions (2.15c, d) are obtained from (2.14) and (2.12b).

The computational scheme to determine $Q^* = Q^*(z)$, and therefore $A^* = A^*(z)$, is as follows. We first truncate (2.15) to a finite domain by imposing the artificial boundary condition $u^{*'} + (r^{-1} + 1)u^* = 0$ at some $r = r_\infty \gg 1$. Then, the resulting problem is solved numerically using the collocation package COLSYS (cf. [1]) for various values of Q^*. The condition (2.15c) then yields z as a function of Q^*. With a specific choice of gauge $\nu(z)$, such as $\nu(z) = -1/\log z$, $A^*(z)$ is obtained from $A^*(z) = Q^*(z)/\nu(z)$. To compare with the hybrid results, COLSYS is also used to compute the curve $Q(\epsilon)$ versus ϵ, at various values of κ, from the full problem (2.1).

In Fig. 1 we compare the full numerical results for $Q(\epsilon)$ with the corresponding hybrid results $Q^*(\epsilon)$, for each of the two forms $f(u) = u$ and $f(u) = 2u^3/(1 + u^2)$, with $\kappa = \infty$ ($d = 1$). The hybrid method is seen to determine accurately $Q(\epsilon)$ up to $\epsilon = 0.150$, being somewhat better for $f(u) = 2u^3/(1 + u^2)$ than for $f(u) = u$. A similar comparison, but over a wider range of ϵ, is shown in Fig. 2 for the parameter value $\kappa = 1$ ($d = e^{-1}$). For $f(u) = 2u^3/(1 + u^2)$ with $\kappa = \infty$, in Fig. 3 we compare the hybrid results for $Q(\epsilon)$ with the two, three and four-term truncated series obtained from (2.8) and (2.9) with $\nu(z) = -1/\log z$. When $f(u) = u$ and $\kappa = 1$, similar results are given in Table 1. We have carried out similar comparisons between the results from the hybrid method, the full problem, and the truncated asymptotic series for other values of κ. In almost all of the cases we have considered, the hybrid method provides a significantly better determination of $Q(\epsilon)$ than does the truncated asymptotic series. However, for $f(u) = u$ and $\kappa = \infty$, the three-term asymptotic series for $Q(\epsilon)$ performs somewhat better than the hybrid method over the range $0.23 < \epsilon < 0.35$, although this is probably fortuitous.

There are two advantages in solving the hybrid problem (2.15) instead of the full problem (2.1). Firstly, (2.15) is not as stiff as (2.1) near $z = 0$. However, the primary advantage is that once the curve $Q^* = Q^*(z)$ is determined, it can be used for any $\kappa > 0$ without any additional computations. A similar universality feature will occur in §3 when calculating the drag coefficient for low Reynolds number flow around a cylinder.

A related hybrid approach can be used to sum logarithmic expansions that occur for other nonlinear problems, including

$$u'' + \frac{1}{r}u' + f(u) = 0, \quad 0 < \epsilon \le r \le 1, \tag{2.16a}$$

$$\epsilon u'(\epsilon) - \kappa u(\epsilon) = 0, \qquad u(1) = 0. \tag{2.16b}$$

In analogy with (2.12), the 'flux' $Q(\epsilon) \equiv \epsilon u'(\epsilon)$ for (2.16) is given asymptotically, to within all logarithmic correction terms, by $Q(\epsilon) = Q^*(\epsilon d) + \cdots$ as $\epsilon \to 0$. Here $d = e^{-1/\kappa}$ and $Q^*(z)$ is determined in terms of the solution to the related problem

$$u_H'' + \frac{1}{r} u_H' + f(u_H) = 0\,, \quad 0 < r \leq 1\,, \tag{2.17a}$$

$$u_H(1) = 0\,, \qquad u_H = Q^*(z)\,[\log r - \log z] + o(1)\,, \quad r \to 0\,. \tag{2.17b}$$

In general, $Q^*(z)$ can only be obtained numerically. However, for the case of an exponential nonlinearity where $f(u) = e^u$, the asymptotic validity of the hybrid formulation (2.17) can be verified analytically by calculating certain explicit solutions from (2.16) and (2.17) (see [19]).

In [3] a different method was used to solve Lagerstrom's version of (2.1). The gauge function $-1/\log\epsilon$ was replaced by $1/E_1(\epsilon)$ and an iteration process was employed requiring that the outer corrections *exactly* satisfy the boundary condition $u(\epsilon) = 0$. By satisfying the boundary condition exactly, such an iteration approach provides a more accurate approximation of the solution to Lagerstrom's problem than does the hybrid method. For more general problems, such as flow past a cylinder, a numerical solution for each iterate would be required where each iterate satisfies the exact boundary condition on the cylinder. However, this would involve nearly the same amount of work as solving the full problem numerically. Moreover, when the cross-sectional shape of the cylinder is changed, the iterative approach would require a complete re-calculation of the flow field and the drag coefficient. We now show that with the hybrid approach results are obtained that can be used for cylinders of different cross-sectional shapes with only a minimal amount of extra computation.

3. The Logarithmic Expansion for Slow Viscous Flow

Now we consider steady, incompressible, viscous flow around a cylindrical body with a uniform stream of velocity U_∞ in the x direction at large distances from the body. We assume that the cross-section D_0 of the cylinder is star-shaped and, for simplicity, we assume that D_0 is symmetric with respect to the oncoming stream. Then, in terms of polar coordinates centered inside the body, it follows from the Navier-Stokes equations that the dimensionless stream function ψ satisfies

$$\nabla^4\psi + \epsilon\, J_r\big[\psi, \nabla^2\psi\big] = 0\,, \quad \text{for} \quad r > r_b(\theta)\,, \tag{3.1a}$$

$$\psi = \partial_n\psi = 0\,, \quad \text{on} \quad r = r_b(\theta)\,, \tag{3.1b}$$

$$\psi \sim y\,, \quad \text{as} \quad r = (x^2 + y^2)^{1/2} \to \infty\,. \tag{3.1c}$$

Here $\epsilon \equiv U_\infty L/\nu \ll 1$ is the Reynolds number based on the radius L of D_0, lengths are in units of L, ∂_n denotes the normal derivative, and J_r is the Jacobian defined by $J_r\big[a, b\big] \equiv r^{-1}\,(\partial_r a\,\partial_\theta b - \partial_\theta a\,\partial_r b)$. The boundary of the scaled cross-section is denoted by $r = r_b(\theta)$ for $-\pi \leq \theta \leq \pi$ and the symmetry condition $r_b(\theta) = r_b(-\theta)$ is assumed to hold. In terms of ψ, the dimensionless negative vorticity ω and the x and y components of the fluid velocity, u and v, are

$$u = \partial_y\psi = \sin\theta\,\partial_r\psi + \frac{\cos\theta}{r}\,\partial_\theta\psi\,, \quad v = -\partial_x\psi = -\cos\theta\,\partial_r\psi + \frac{\sin\theta}{r}\,\partial_\theta\psi\,, \quad \omega = \nabla^2\psi\,. \tag{3.2}$$

We now briefly outline the conventional singular perturbation analysis of (3.1) for $\epsilon \to 0$ (cf. [5], [12]), and we formulate the hybrid method for summing the infinite-order logarithmic expansions that arise from the analysis.

3.1 The Stokes Expansion

In the Stokes region, defined by $r = O(1)$, the stream function has an infinite logarithmic expansion of the form

$$\psi_s(r,\theta) = \sum_{j=1}^{\infty} \nu^j(z)\psi_j(r,\theta) + \cdots . \tag{3.3}$$

Here $\nu(z) \equiv -1/\log(ze^{1/2})$ and $z \equiv \epsilon d$, where d is specified below. Substituting (3.3) into (3.1a), we obtain that $\psi_j = a_j\psi_c$, where the a_j for $j = 1, 2, ..$ are undetermined constants and $\psi_c \equiv \psi_c(r,\theta)$ is the solution to the following canonical problem:

$$\nabla^4\psi_c = 0\,, \quad \text{for} \;\; r > r_b(\theta)\,; \qquad \psi_c(r,\theta) = -\psi_c(r,-\theta)\,, \tag{3.4a}$$

$$\psi_c = 0 \quad \text{and} \quad \partial_n\psi_c = 0\,, \quad \text{upon} \;\; r = r_b(\theta)\,. \tag{3.4b}$$

The asymptotic form of ψ_c as $r \to \infty$ involves linear combinations of $\left\{r^3, r\log r, r, r^{-1}\right\}\sin\theta$. To match ψ_s with the Oseen expansion (see §3.2 below), the coefficient of r^3 must vanish. Then, to specify ψ_c uniquely, we impose that the coefficient of $r\log r$ is unity. Thus, we define ψ_c as the unique solution to (3.4a,b) that satisfies

$$\psi_c \sim \left(r\log r - r\log[de^{1/2}]\right)\sin\theta\,, \quad \text{as} \;\; r \to \infty\,. \tag{3.4c}$$

The form (3.4c) relies on the assumption that the cylinder is symmetric with respect to the oncoming stream. The constant d in (3.4c), which depends on the shape of the body, is determined uniquely by the solution to (3.4). Substituting $\psi_j = a_j\psi_c$ into (3.3) gives the Stokes expansion

$$\psi_s(r,\theta) = \sum_{j=1}^{\infty} \nu^j(z)\, a_j\psi_c(r,\theta) + \cdots , \tag{3.5a}$$

and (3.4c) shows that it has the following far-field behavior:

$$\psi_s(r,\theta) \sim \sum_{j=1}^{\infty} \nu^j(z)\, a_j \left(r\log r - r\log[de^{1/2}]\right)\sin\theta\,, \quad \text{as} \;\; r \to \infty\,. \tag{3.5b}$$

3.2 The Oseen Expansion

In the Oseen region, defined by $r = O(\epsilon^{-1})$, we introduce new variables ρ and Ψ by $\rho = \epsilon r$ and $\Psi(\rho,\theta) = \epsilon\psi(\epsilon^{-1}\rho,\theta)$, and we expand Ψ as

$$\Psi(\rho,\theta) = \rho\sin\theta + \nu(z)\Psi_1(\rho,\theta) + \sum_{j=2}^{\infty} \nu^j(z)\Psi_j(\rho,\theta) + \cdots . \tag{3.6}$$

Substituting (3.6) into (3.1) and matching Ψ as $\rho \to 0$ to the far-field form of the Stokes expansion given in (3.5b), we find that $a_1 = 1$ and that Ψ_1 and Ψ_j, for $j = 2, 3..$, satisfy the following equations on $0 < \rho < \infty$:

$$L_{0s}\Psi_1 \equiv \nabla^4\Psi_1 + \left(\rho^{-1}\sin\theta\,\partial_\theta - \cos\theta\,\partial_\rho\right)\nabla^2\Psi_1 = 0\,, \tag{3.7a}$$

$$\Psi_1 \sim (\log\rho + a_2)\,\rho\sin\theta\,, \quad \text{as} \quad \rho \to 0\,; \quad \partial_\rho\Psi_1 \to 0\,, \quad \text{as} \quad \rho \to \infty\,, \tag{3.7b}$$

$$L_{0s}\Psi_j = -\sum_{k=1}^{j-1} J_\rho\big[\Psi_k, \nabla^2\Psi_{j-k}\big]\,, \tag{3.8a}$$

$$\Psi_j \sim (a_j\log\rho + a_{j+1})\,\rho\sin\theta\,, \quad \text{as} \quad \rho \to 0\,; \quad \partial_\rho\Psi_j \to 0\,, \quad \text{as} \quad \rho \to \infty\,. \tag{3.8b}$$

Here L_{0s} is the linearized Oseen operator and Ψ_1 is the linearized Oseen solution.

The constants a_j for $j = 2, 3, ..$, which are independent of ϵ and of the shape of the body, are determined recursively from (3.7) and (3.8). The first two coefficients are

$$\begin{aligned} a_2 &= \gamma - \log 4 - 1 \approx -1.8091\,, \\ a_3 - a_2^2 &= -\int_0^\infty \left[r^{-1}I_1(2r) + 1 - 4K_1(r)I_1(r)\right] K_0(r)K_1(r)\,dr \approx -0.8669\,. \end{aligned} \tag{3.9}$$

Here K_1, K_0, I_0 and I_1 are modified Bessel functions, and γ is Euler's constant. This formula for a_2 was obtained in [5] and [12] and the expression for a_3 was given in [5] (see Appendix B). Explicit analytical formulae for a_j when $j \geq 4$ are not available. For $\epsilon \to 0$, the drag coefficient C_D for a cylinder of arbitrary cross-section is given in terms of the a_j by (see Appendix B)

$$C_D \sim 4\pi\epsilon^{-1}\nu(\epsilon d)\big(\sum_{j=0}^{\infty} a_{j+1}\nu^j(\epsilon d) + \cdots\big)\,. \tag{3.10a}$$

Kaplun's [5] approximation for C_D results from substituting $a_1 = 1$ and (3.9) into (3.10a). The three-term expansion can be written as

$$C_D \sim 4\pi\epsilon^{-1}\hat{\nu}(\epsilon d)\left[1 - 0.8669\,\hat{\nu}^2(\epsilon d)\right]\,, \qquad \hat{\nu}(z) \equiv \left[\log\left(3.7027/z\right)\right]^{-1}\,. \tag{3.10b}$$

For a circular cylinder, the explicit form (3.10b) provides a poor determination of the experimental drag coefficient unless ϵ is rather small (cf. [18]). One way to overcome this difficulty would be to compute numerically further coefficients a_j, for $j \geq 4$, from the the infinite sequence of partial differential equations (3.8). This would still require truncating the series (3.10a) at some finite j. As an alternative to series truncation, we now formulate a hybrid asymptotic-numerical method that has the effect of summing all the terms on the right side of (3.10a), but which avoids computing the a_j.

3.3 The Hybrid Formulation

Let $A^*(z)$ denote a function which is asymptotic to the sum of the terms written explicitly in the brackets on the right side of (3.10a),

$$A^*(z) \sim \sum_{j=1}^{\infty} \nu^{j-1}(z)\,a_j\,. \tag{3.11}$$

Then, the Stokes expansion (3.5a) is asymptotic to

$$\psi_s(r,\theta) = \nu(\epsilon d) A^*(\epsilon d)\psi_c(r,\theta) + \cdots . \tag{3.12}$$

Substituting (3.4c) into (3.12) and expressing the result in terms of the Oseen variable $\rho = \epsilon r$, we obtain the far-field form

$$\psi_s \sim \epsilon^{-1}\rho\sin\theta\, A^*(z)\,[1 + \nu(z)\,\log\rho] \,. \tag{3.13}$$

To determine $A^*(z)$, we then solve (3.1a,c) for $\rho > 0$ (where $\rho = \epsilon r$), subject to the singularity condition (3.13), which is to hold as $\rho \to 0$. Therefore, we obtain the following related problem for $A^*(z)$ and the auxiliary function $\Psi_H \equiv \Psi_H(\rho,\theta;z)$:

$$\nabla^4\Psi_H + J_\rho\big[\Psi_H, \nabla^2\Psi_H\big] = 0\,, \qquad \rho > 0\,; \qquad \Psi_H(\rho,\theta;z) = -\Psi_H(\rho,-\theta;z)\,, \tag{3.14a}$$

$$\Psi_H \sim \rho\sin\theta\,, \quad \text{as} \quad \rho\to\infty\,, \tag{3.14b}$$

$$\Psi_H = \rho\sin\theta\,[1 + \nu(z)\log\rho]\; A^*(z) + o(\rho)\,, \quad \text{as} \quad \rho\to 0\,. \tag{3.14c}$$

Here $\nu(z) = -1/\log(ze^{1/2})$. When z is sufficiently small, the problem (3.14a,b) with $\Psi_H \to A^*\nu\rho\log\rho\sin\theta$ as $\rho\to 0$ is solvable for any A^*. However, the extra condition in (3.14c) that $\Psi_H - A^*\nu\rho\log\rho\sin\theta \to A^*\rho\sin\theta$ as $\rho\to 0$, provides an equation for A^*. By expanding the solution to (3.14) in powers of $\nu(z)$, we find that Ψ_H and A^* are asymptotic to the sums of the terms written on the right hand sides of (3.6) and (3.11), respectively. We also note that $A^*\to 1$ as $z\to 0$.

The related problem (3.14) is a hybrid asymptotic-numerical formulation of the full problem (3.1). More specifically, the cylinder in (3.1) is replaced by the singularity structure (3.14c) that was derived by exploiting the far-field form of the infinite-order logarithmic expansion in the Stokes region. We then are left with having to compute the solution to the parameter-dependent problem (3.14), rather than having to compute the solutions to the infinite sequence of problems (3.7), (3.8). In terms of A^* and d, the asymptotic formula for the drag coefficient, valid to within all logarithmic correction terms, is given by

$$C_D = 4\pi\epsilon^{-1}\left[\nu(\epsilon d)A^*(\epsilon d) + \cdots\right], \qquad \nu(\epsilon d) = -1/\log\big(\epsilon d\, e^{1/2}\big)\,. \tag{3.15}$$

Kaplun's equivalence principle follows from the fact that the curve $A^*(z)$ versus z can be used for a cylinder of arbitrary cross-section. To determine $A^*(\epsilon d)$ for a body of a specific shape, we need only compute the *single constant* d from the numerical solution to the canonical Stokes problem (3.4). This feature provides a significant advantage over a direct numerical approach on the full problem (3.1).

For some special cross-sectional shapes, the constant d, defined from (3.4), can be determined analytically. For a circular cross-section with $r_b(\theta) = 1$,

$$\psi_c = \left(r\log r - \frac{r}{2} + \frac{1}{2r}\right)\sin\theta\,, \qquad d = 1\,. \tag{3.16}$$

Next we consider an elliptical domain defined by $(x/a)^2 + (y/b)^2 = 1$ where $\max(a, b) = 1$. In the case where $a = 1$ (the major axis is aligned parallel to the oncoming stream), the solution to (3.4) is

$$\psi_c = \beta \sinh\xi \, \sin\eta \left(\xi - \xi_0 + \frac{b^2}{\beta^2} \coth\xi - \frac{ab}{\beta^2} \right) . \tag{3.17}$$

Here ξ, η, β, and ξ_0 are defined by

$$x = \beta \cosh\xi \cos\eta \,, \quad y = \beta \sinh\xi \sin\eta \,, \quad \beta = \left(a^2 - b^2\right)^{1/2} \,, \quad \xi_0 = \frac{1}{2} \log\left(\frac{a+b}{a-b} \right) . \tag{3.18}$$

Thus d is given by

$$d = \left(\frac{a+b}{2} \right) \exp\left[\frac{b-a}{2(b+a)} \right] . \tag{3.19}$$

This formula for d also holds for the case when $b = 1$ (the major axis is is aligned perpendicular to the oncoming stream). A plot of d for various ellipses is shown in Fig. 4.

4. The Numerical Methods

We now discuss the numerical methods used to calculate the shape-dependent parameter d and to solve the hybrid formulation (3.14). The method used to compute the flow around a circular cylinder from the full problem (3.1) is also outlined.

4.1 The Calculation of the Shape-Dependent Parameter d

For the majority of cross-sectional profiles, analytical solutions to the inner (Stokes) problem (3.4) are not available. We now compute the solution to (3.4) for a given profile C by finite differences to find the corresponding value of the constant d. We first determine a conformal mapping that takes the domain exterior to C to the interior of a unit disc, and we then transform (3.4) accordingly. This allows the boundary conditions (3.4b) to be applied in a straightforward manner. Since the far-field form (3.4c) is transformed to a singularity at the origin of the mapped plane, we modify the stream function ψ_c by removing from it the required singular behavior. A finite-difference scheme is then used to solve for this modified stream function. Finally, the shape-dependent parameter d is found from matching the behaviour of the stream function near the origin to (3.4c).

In (3.4), the profile C is given in terms of polar coordinates (r, θ) by $r = r_b(\theta)$ for $-\pi \le \theta \le \pi$, where $\max_\theta |r_b(\theta)| = 1$ and $r_b(\theta) = r_b(-\theta)$. Let $z = re^{i\theta}$. Then by Riemann's mapping theorem, there exists a one-to-one map $z \to \zeta$ such that the profile C is transformed to the unit circle in the ζ plane, and the two exterior planes correspond. By a further mapping $\zeta = 1/\sigma$, the unbounded domain becomes the computationally more tractable interior unit disc, given by $\sigma = \rho \exp(i\vartheta)$ with $\rho < 1$. Under the transformation $z \to \sigma$, (3.4a, b) becomes in the (ρ, ϑ) variables

$$\nabla^2 \left(B^{-2} \nabla^2 \psi_c \right) = 0 \,, \quad 0 < \rho < 1 \,; \qquad B = B(\rho, \vartheta) \equiv |dz/d\sigma| \,, \tag{4.1a}$$

$$\psi_c = \partial_\rho \psi_c = 0 \,, \quad \text{on} \quad \rho = 1 \,. \tag{4.1b}$$

The far-field behavior $r \to \infty$ in (3.4c) corresponds to $\rho \to 0$ in the σ plane. For $\sigma \to 0$, the conformal mapping has the form $z \sim \beta_0/\sigma + \beta_1 + \cdots$. This mapping is determined uniquely from the normalization

$\max_\theta |r_b(\theta)| = 1$, which fixes a value for the constant β_0. Thus, $r \sim \beta_0/\rho$, $\theta \sim -\vartheta$, and $B^2 \sim \beta_0 \rho^{-4}$ as $\sigma \to 0$. Therefore, (3.4c) transforms to

$$\psi_c \sim \beta_0 \rho^{-1} \left[\log \rho + \log \left(d e^{1/2} \beta_0^{-1} \right) \right] \sin \vartheta \,, \quad \text{as} \quad \rho \to 0 \,. \tag{4.1c}$$

To solve the transformed problem (4.1), it is convenient to decompose ψ_c as

$$\psi_c = \beta_0 \rho^{-1} \log \rho \, \sin \vartheta + \rho^{-1} \psi^* \,. \tag{4.2}$$

Then, from (4.1c), we have that ψ^* is regular at the origin and satisfies $\partial_\rho \psi^* \to 0$ as $\rho \to 0$. Substituting (4.2) into (4.1) and exploiting the symmetry of the flow field, we can write the problem for ψ^*, defined in the domain $(\rho, \vartheta) \in [0,1] \times [0, \pi]$, in the following stream function-vorticity form:

$$\partial_\rho \left(\rho^{-1} \partial_\rho \psi^* \right) + \rho^{-3} \left(\psi^* + \partial_{\vartheta\vartheta} \psi^* \right) = B^2 \omega + 2 \beta_0 \rho^{-3} \sin \vartheta \,; \qquad \nabla^2 \omega = 0 \,, \tag{4.3a}$$

$$\psi^* = 0 \,, \qquad \partial_\rho \psi^* = -\beta_0 \sin \vartheta \,, \quad \text{on} \quad \rho = 1 \,; \qquad \partial_\rho \psi^* \to 0 \,, \quad \text{as} \quad \rho \to 0 \,. \tag{4.3b}$$

$$\psi^*(\rho, 0) = \omega(\rho, 0) = \psi^*(\rho, \pi) = \omega(\rho, \pi) = 0 \,. \tag{4.3c}$$

From (4.1c) and (4.2), we find that the constant d is determined from the solution to (4.3) by

$$\psi^* \sim \beta_0 \log \left(d e^{1/2} \beta_0^{-1} \right) \sin \vartheta \,, \quad \text{as} \quad \rho \to 0 \,. \tag{4.4}$$

Assume that the conformal map $z = z(\sigma)$, and hence $B(\rho, \vartheta)$ and β_0 in (4.3), are known. (Finding a suitable mapping is a nontrivial problem and is not considered here. The reader is referred to [10], [17] for a discussion on methods for numerical conformal mapping). We now outline the finite-difference scheme used for (4.3). A uniform polar grid is introduced, and the intersection of the grid lines are positioned at $(\rho_i, \vartheta_j) = ((i - 1/2)\Delta\rho, j\Delta\vartheta)$, where $\Delta\rho = 1/(N - 1/2)$ and $\Delta\vartheta = \pi/M$. Here $N + 1$ and $M + 1$ are the number of grid lines in the ρ and ϑ directions, respectively. Note also that the grid has been aligned so that the grid points straddle the origin but otherwise lie on the boundary of the computational domain. Let the unknown $\psi^*_{i,j}$ and $\omega_{i,j}$ approximate $\psi^*(\rho_i, \vartheta_j)$ and $\omega(\rho_i, \vartheta_j)$, respectively. Using a centered, second-order accurate discretization, we obtain the following discrete forms for (4.3a):

$$\begin{aligned} \frac{1}{\Delta\rho} \left[\frac{1}{\rho_{i+1/2}} \frac{(\psi^*_{i+1,j} - \psi^*_{i,j})}{\Delta\rho} - \frac{1}{\rho_{i-1/2}} \frac{(\psi^*_{i,j} - \psi^*_{i-1,j})}{\Delta\rho} \right] + \frac{1}{\rho_i^3} \psi^*_{i,j} \\ + \frac{\left(\psi^*_{i,j+1} - 2\psi^*_{i,j} + \psi^*_{i,j-1} \right)}{\rho_i^3 (\Delta\vartheta)^2} - B^2_{i,j} \, \omega_{i,j} = \frac{2\beta_0}{\rho_i^3} \sin \vartheta_j \,, \\ \frac{1}{\Delta\rho} \frac{1}{\rho_i} \left[\rho_{i+1/2} \frac{(\omega_{i+1,j} - \omega_{i,j})}{\Delta\rho} - \rho_{i-1/2} \frac{(\omega_{i,j} - \omega_{i-1,j})}{\Delta\rho} \right] \\ + \frac{(\omega_{i,j+1} - 2\,\omega_{i,j} + \omega_{i,j-1})}{\rho_i^2 (\Delta\vartheta)^2} = 0 \,, \end{aligned} \tag{4.5a}$$

for $1 \le i \le N - 1$, $1 \le j \le M - 1$. The boundary conditions (4.3b, c) are discretized as

$$\psi^*_{1,j} - \psi^*_{0,j} = \psi^*_{N,j} = 0 \,, \qquad \psi^*_{N+1,j} - \psi^*_{N-1,j} = -2\beta_0 \Delta\rho \sin \vartheta_j \,, \qquad 1 \le j \le M - 1 \,, \tag{4.5b}$$

$$\psi^*_{i,0} = \psi^*_{i,M} = \omega_{i,0} = \omega_{i,M} = 0 \,, \qquad 1 \le i \le N + 1 \,. \tag{4.5c}$$

Consistent boundary conditions for ω at the origin and at $\rho = 1$, which are derived from (4.3a), are

$$\begin{aligned} \omega_{1,j} - \omega_{0,j} &= 0\,, \qquad 1 \le j \le M-1\,, \\ B_{N,j}^2\,\omega_{N,j} - \frac{\left(\psi^*_{N+1,j} - 2\psi^*_{N,j} + \psi^*_{N-1,j}\right)}{(\Delta\rho)^2} &= -\beta_0 \sin\vartheta_j\,, \qquad 1 \le j \le M-1\,. \end{aligned} \tag{4.5d}$$

In matrix form, the discrete problem (4.5) is a sparse linear system for the unknowns $\psi^*_{i,j}$ and $\omega_{i,j}$, and is solved using the sparse matrix solver of [6]. Once a numerical solution has been obtained, the constant d is calculated by fitting the numerical solution to the form (4.4) as follows:

$$d = \beta_0\,\exp\left[\beta_0^{-1}\psi^*_{av} - 1/2\right]\,, \quad \text{where} \quad \psi^*_{av} \equiv \frac{1}{M-1}\sum_{j=1}^{M-1}\frac{\left(\psi^*_{1,j} + \psi^*_{0,j}\right)}{2\sin\vartheta_j}\,. \tag{4.6}$$

(The computations show that the agreement between the numerical solution and the asymptotic form (4.4) is excellent. The typical range of values of $(\psi^*_{1,j} + \psi^*_{0,j})/(2\sin\vartheta_j)$ for $1 \le j \le M-1$ on a 40×40 mesh is roughly 10^{-4}).

This computational method was first tested on ellipses of various aspect ratios, and the calculated values of d were compared to the analytical formula (3.19). The numerical and analytical results were in excellent agreement: on a 40×40 mesh, the error was on the order of 10^{-4}. An interesting example for which an analytical conformal mapping is known is the family of symmetric Karman-Trefftz airfoils (cf. [11]). The mapping function $z = z(\sigma)$ for these profiles is

$$z(\sigma) = \beta_0 kc\left[\frac{(\xi+c)^k + (\xi-c)^k}{(\xi+c)^k - (\xi-c)^k}\right]\,, \qquad \xi \equiv 1/\sigma + c - 1\,, \tag{4.7a}$$

where $\sigma = \rho e^{i\vartheta}$. By fixing the length of the airfoil to be 2, we find that the mapping constant β_0 is given in terms of k and c by

$$\beta_0 = \frac{[1-(1-c)^k]}{kc}\,. \tag{4.7b}$$

A parametric representation for the airfoil profile is obtained by setting $\sigma = e^{i\vartheta}$ in (4.7a). In (4.7), the parameters k and c, where $1 < k < 2$ and $0 < c < 1$, determine the thickness ratio δ of the airfoil and the tail angle θ_T, given by $\theta_T = (2-k)\pi$. Although the mapping is known analytically for these profiles, the constant d must be calculated numerically from (4.5). As an example, when $k = 1.91$ and $c = .954$, the airfoil characteristics are $\delta = 0.12$ and $\theta_T = 16^\circ$. For this case, we calculate from (4.5) and (4.6) that $d = 0.364$. The corresponding inner Stokes solution ψ_c and the vorticity ω are shown in Fig. 5. Numerical values for d for other Karman-Trefftz airfoils are given in Table 2.

4.2 The Numerical Solution of the Outer Hybrid Problem

We now discuss the numerical solution of the parameter-dependent problem (3.14). Because of the unboundedness of Ψ_H as $\rho \to \infty$ and the singularity structure near $\rho = 0$, it is convenient to first decompose the solution to (3.14) as

$$\Psi_H(\rho,\theta;z) = \rho\sin\theta + \kappa(z)\Psi_1(\rho,\theta) + \Psi^*(\rho,\theta;z)\,. \tag{4.8}$$

Here $\kappa(z) \equiv A^*(z)\nu(z)$ and Ψ_1 satisfies (3.7). Substituting (4.8) into (3.14), we obtain that Ψ^* is regular as $\rho \to 0$ and satisfies

$$L_{0s}\Psi^* = -J_\rho\left[\kappa(z)\Psi_1 + \Psi^*, \kappa(z)\nabla^2\Psi_1 + \nabla^2\Psi^*\right], \qquad \rho > 0\,, \tag{4.9a}$$

$$\partial_\rho\Psi^* \to 0\,, \quad \text{as} \quad \rho \to \infty\,; \qquad \Psi^*(\rho,\theta;z) = -\Psi^*(\rho,-\theta;z)\,, \tag{4.9b}$$

$$\Psi^* = \rho\left[A^*(z) - 1 + \kappa(z)\left(\log 4 + 1 - \gamma\right)\right]\sin\theta + o(\rho)\,, \quad \text{as} \quad \rho \to 0\,. \tag{4.9c}$$

In (4.9c), γ is Euler's constant. We solve (4.9) for various values of κ to obtain A^* as a function of κ. Then, by computing z from $\nu(z) = \kappa/A^*$ and $\nu(z) = -1/\log(ze^{1/2})$, we obtain the curve $A^*(z)$ versus z. Finally, setting $z = \epsilon d$, where the shape parameter d is computed as in §4.1, the curve C_D versus ϵ is found from (3.15).

To solve (4.9), we first introduce a mapping function. Since the modified stream function Ψ^* on the unbounded domain is expected to decay slowly as $\rho \to \infty$, it is not appropriate to map the unbounded domain to a bounded domain as was done in §4.1; with such a mapping, the far-field stiffness would be difficult to resolve numerically. Instead, a logarithmic radial stretching function, $\tau = \log(1+\rho)$, is introduced. This stretching function is analogous to the change of coordinates used in [2] and [15] in their calculations on the full incompressible Navier-Stokes equations for flow around a circular cylinder. In terms of this new radial coordinate, the domain is now $\tau > 0$, $0 \le \theta \le \pi$, and (4.9) becomes

$$\tilde{L}_{0s}\omega^* + \frac{e^\tau}{e^\tau - 1}\tau J_\tau\left(\kappa\Psi_1 + \Psi^*,\, \kappa\nabla^2\Psi_1 + \omega^*\right) = 0\,; \qquad \tilde{\nabla}^2\Psi^* = e^{2\tau}\omega^*\,, \tag{4.10a}$$

$$\Psi^*(\rho,0) = \Psi^*(\rho,\pi) = \omega^*(\rho,0) = \omega^*(\rho,\pi) = 0\,; \qquad \partial_\rho\Psi^* \to 0\,, \quad \text{as} \quad \tau \to \infty\,, \tag{4.10b}$$

$$\Psi^* \to (e^\tau - 1)\left[A^* - 1 + \kappa(\log 4 + 1 - \gamma)\right]\sin\theta\,, \quad \text{as} \quad \tau \to 0\,. \tag{4.10c}$$

Here $\tilde{L}_{0s}$ and $\tilde{\nabla}^2$ are defined by

$$\begin{aligned} \tilde{\nabla}^2 &\equiv \frac{e^\tau}{e^\tau - 1}\,\frac{\partial}{\partial\tau}\left(\frac{e^\tau - 1}{e^\tau}\,\frac{\partial}{\partial\tau}\right) + \left(\frac{e^\tau}{e^\tau - 1}\right)^2\,\frac{\partial^2}{\partial\theta^2}\,, \\ \tilde{L}_{0s} &\equiv \tilde{\nabla}^2 + e^\tau\left(\frac{e^\tau}{e^\tau - 1}\sin\theta\frac{\partial}{\partial\theta} - \cos\theta\frac{\partial}{\partial\tau}\right)\,. \end{aligned} \tag{4.10d}$$

The transformed problem (4.10) is now in a form suitable for solution by finite differences. Introducing a finite outer limit τ_∞, the computational grid is defined by the grid points $(\tau_i, \theta_j) = (i\Delta\tau, j\Delta\theta)$, where $\Delta\tau = \tau_\infty/(N + 1/2)$ and $\Delta\theta = \pi/M$. On this grid, (4.10) is discretized in the same manner as (4.3), and the resulting system of nonlinear equations is solved using Newton's method. We will not discuss this in detail. Instead, we focus on the numerical resolution of two potential difficulties: the singular behavior of the coefficients in (4.10a) near the origin and the far-field behavior at the artificial boundary $\tau = \tau_\infty$. From (4.10c), the discrete unknowns $\Psi^*_{0,j}$ and $\omega^*_{0,j}$ at the origin are set to zero. The difference operators for the governing equations are then applied to the interior grid points, starting at the first grid line $\tau = \Delta\tau$. Although the derivatives of the Oseen solution in the Jacobian J_τ are unbounded at the origin, their forms

are known analytically (see Appendix B) and therefore can be evaluated precisely at all needed points. This discretization results in a well-behaved difference operator near the origin, even as the finite-difference mesh is refined. The second difficulty is the choice of an appropriate artificial far-field boundary condition at $\tau = \tau_\infty$. Based on the work in [2], the approximate Neumann conditions $\Psi^*_{N+1,j} - \Psi^*_{N,j} = \omega^*_{N+1,j} - \omega^*_{N,j} = 0$ are used to achieve the appropriate far-field decay.

Once a solution to the discrete system is obtained, its behavior is matched near the origin according to (4.10c). First note that at $\tau = \Delta\tau/2$, $\theta = \theta_j$, we have

$$\frac{\partial \Psi^*}{\partial \tau} \approx \frac{\Psi^*_{1,j}}{\Delta\tau} \approx e^{\Delta\tau/2}\,\left[A^* - 1 + \kappa(\log 4 + 1 - \gamma)\right] \sin\theta_j. \tag{4.11}$$

This condition then gives a range of constants

$$A^*_j = \left(\frac{e^{-\Delta\tau/2}}{\sin\theta_j}\right)\left(\frac{\Psi^*_{1,j}}{\Delta\tau}\right) + 1 - \kappa\left(\log 4 + 1 - \gamma\right). \tag{4.12}$$

From $\nu(z) = \kappa/A^*$ and $\nu(z) = -1/\log(ze^{1/2})$, we then obtain a range of corresponding z values. The variation in this range is an indication of both the numerical resolution and the validity of the asymptotic approximation (see §5 below).

4.3 The Numerical Solution of the Exact Problem for Flow Past a Cylinder

To compare the performance of our hybrid method, we solve the exact equations (3.1), defined on $r > 1$, $0 \le \theta \le \pi$, for the case of a circular cylinder. To solve (3.1) we decompose the stream function as $\psi = r\sin\theta + \psi^*$ and we introduce the stretching function $\tau = \log r$. Then, in the transformed domain $\tau > 0$, $0 \le \theta \le \pi$, (3.1) becomes

$$\tilde{L}_{ex}\,\omega + \epsilon\tau J_\tau(\psi^*, \omega) = 0\,; \qquad \tilde{\nabla}^2\psi^* = e^{2\tau}\omega\,, \tag{4.13a}$$

$$\psi^* = \partial_\tau\psi^* = -\sin\theta\,, \quad \text{on} \;\; \tau = 0; \qquad \partial_\tau\psi^*\,,\; \partial_\tau\omega \to 0\,, \quad \text{as} \;\; \tau \to \infty\,, \tag{4.13b}$$

$$\psi^*(\tau,0) = \psi^*(\tau,\pi) = \omega(\tau,0) = \omega(\tau,\pi) = 0\,. \tag{4.13c}$$

Here

$$\tilde{\nabla}^2 \equiv \frac{\partial^2}{\partial\tau^2} + \frac{\partial^2}{\partial\theta^2}\,; \qquad \tilde{L}_{ex} \equiv \tilde{\nabla}^2 + \epsilon\, e^{\tau}\left(\sin\theta\frac{\partial}{\partial\theta} - \cos\theta\frac{\partial}{\partial\tau}\right). \tag{4.13d}$$

To solve (4.13) numerically we use the same finite-difference grid and artificial far-field decay conditions as was used for computing solutions to the hybrid formulation. Once a solution has been obtained for a given ϵ, the drag coefficient is calculated from (B.8). Using the trapezoid rule to approximate the integral in (B.8) and replacing ω_r by a one-sided difference quotient, we obtain

$$C_D = 2\,\epsilon^{-1}\sum_{j=1}^{M-1}\left(\omega_{0,j} - \frac{4\omega_{1,j} - 3\omega_{0,j} - \omega_{2,j}}{2\Delta\tau}\right)\Delta\theta\sin\theta_j\,. \tag{4.14}$$

5. Results and Discussion

Using the numerical method of §4.2, the solution to the outer hybrid problem (4.10) is computed on a 120×120 mesh with the artificial boundary condition imposed at $\tau_\infty = 60$. In the absence of any discretization error, the asymptotic theory indicates that as $z \to 0$ ($\kappa \to 0$) the constants A_j^*, for $j = 1, ..,$ in (4.12) should be independent of j. However, as a result of the discretization errors incurred in solving (4.10) and the errors in the asymptotic theory resulting from using the hybrid formulation at finite values of κ, the computations yielded a narrow range of constants A_j^*. For each fixed κ, let A_{min}^* and A_{max}^* denote the minimum and the maximum values of the A_j^* for $j = 1, 2, ...$ The corresponding values of z are denoted by $\log\left(z_{min}e^{1/2}\right) = -A_{min}^*/\kappa$ and $\log\left(z_{max}e^{1/2}\right) = -A_{max}^*/\kappa$. In this way, we obtain from (3.15) two hybrid drag curves: one corresponding to A_{min}^* and the other to A_{max}^*. The difference between these two curves gives a measure of the 'error bounds' for our hybrid asymptotic-numerical approach.

We now compare the hybrid results for the drag coefficient of a circular cylindrical body for which $d = 1$ and $z = \epsilon$. In Fig. 6 we plot the hybrid drag curves for C_D corresponding to A_{min}^* and to A_{max}^*. In this figure we compare our hybrid results with the three-term expansion (3.10*b*) (with $d = 1$), with the full numerical results computed using the method of §4.3, and with the experimental results of [16]. Notice that the full numerical results for C_D lie within the error bounds associated with the hybrid drag curves. Furthermore, from this figure it is clear that the hybrid method provides a significantly better determination of C_D over the range $0.50 < \epsilon < 2.0$ than does the three-term expansion (3.10*b*). The discrepancy between the full numerical results for C_D and the corresponding experimental values can probably be attributed to the fact that the experimental results were obtained for long but finite cylinders. As shown in [13], the drag coefficient of a long but finite circular cylinder differs rather significantly from that of an infinitely long circular cylinder unless the aspect ratio of the finite cylinder is very small.

In Fig. 7 we show contour plots, in the Stokes variable, of the stream function and the vorticity for the full flow around a circular cylinder at $\epsilon = 0.085$. These results were computed using (4.13). The very slight upstream/downstream asymmetry in the flow field indicates the relative insignificance, at this value of ϵ, of the inertial terms in the Navier-Stokes equations near the cylinder. In Fig. 8 we show contour plots, in the Oseen variable, of the stream function and the vorticity computed from the hybrid problem (4.10) with $\kappa = 0.25$ ($\epsilon \approx 0.085$). This figure compares favorably with the contour plots shown in Fig. 9 of the stream function and the vorticity for the full flow field at $\epsilon = 0.085$ computed using (4.13). In Fig. 10 contour plots for the hybrid stream function and the vorticity are shown at $\kappa = 0.65$ ($\epsilon \approx 1.65$). The corresponding results computed from the full problem with $\epsilon = 1.65$ are shown in Fig. 11. It is interesting that, although the qualitative features of the hybrid and the full flow field become somewhat different as ϵ increases, the hybrid drag coefficient is still very close to the full numerical result even up to $\epsilon = 2.0$.

We now consider flow around other cylindrical bodies. At each fixed κ, we define A_{av}^* by $A_{av}^* = (A_{min}^* + A_{max}^*)/2$ and we define a corresponding value of z by $\log\left(ze^{1/2}\right) = -A_{av}^*/\kappa$. Replacing A^* by A_{av}^* in (3.15) we then obtain a hybrid drag coefficient. By using the values of d given in (3.19) and Table 2, in Fig. 12 we plot this hybrid drag coefficient for flow around certain cylinders having either elliptical or

Karman-Trefftz airfoil cross-sections. In Fig. 13 we compare, for an ellipse and an airfoil, the hybrid results for C_D with the asymptotic result (3.10b).

For each of the Karman-Trefftz airfoil examples given in Table 2, there is an equivalent ellipse with $a = 1$ that has the same value of d. The values of b for these equivalent ellipses, which are computed using (3.19), are given in the last column of Table 2. In particular, an airfoil with thickness ratio $\delta = .20$ and tail angle $\theta_T = 25^\circ$ has the same value of d as an ellipse with $a = 1.0$ and $b = .170$. Each of these equivalent ellipses has the same asymptotic drag coefficient, within all logarithmic correction terms, as the corresponding Karman-Trefftz airfoil. However, it is clear that the transcendentally small terms in the expansion of the drag coefficient, which were not taken into account in our analysis, will not satisfy the same equivalence principle. Work is in progress to calculate these transcendentally small terms.

Acknowledgements

M.J.W. is grateful to Prof. Steve Childress for helpful discussions concerning the work of Kaplun and for his encouragement during the early stages of this work.

REFERENCES

[1] U. Ascher, R. Christiansen, R. Russell, *Collocation Software for Boundary value ODE's,* Math. Comp. 33, (1979), pp. 659-679.

[2] B. Fornberg, *A Numerical Study of Steady Viscous Flow Past a Circular Cylinder*, J. Fluid Mech. 98, (1980), pp. 819-855.

[3] C. Hunter, M. Tajdari, S. D. Boyer, *On Lagerstrom's Model of Slow Incompressible Viscous Flow*, SIAM J. Appl. Math. 50, (1990), pp. 48-63.

[4] I. Imai, *On the Asymptotic Behavior of Viscous Fluid Flow at a Great Distance from a Cylindrical Body, with Special Reference to Filon's Paradox*, Proc. Roy. Soc. A, 208, pp. 487-516.

[5] S. Kaplun, *Low Reynolds Number Flow Past a Circular Cylinder*, J. Math. Mech. Vol. 6, No. 5, (1957), pp. 52-60.

[6] J. R. Kightley, P. A. Forsyth, *MAT1 Iterative Sparse Matrix Solver: User's Guide*, Department of Computer Science, University of Waterloo.

[7] P. A. Lagerstrom, *Matched Asymptotic Expansions*, Applied Mathematical Sciences Vol. 76, Springer-Verlag, New York, (1988).

[8] H. Lamb, *Hydrodynamics*, 6th Ed., Dover Publications Inc., New York, (1945).

[9] S. H. Lee, L. G. Leal, *Low Reynolds Number Flow Past Cylindrical Bodies of Arbitrary Cross-Sectional Shape*, J. Fluid Mech. 164, (1986), pp. 401-427.

[10] R. Menikoff, C. Zemach, *Methods for Numerical Conformal Mapping*, J. Comp. Phys. 36, (1980), pp. 366-410.

[11] L. M. Milne-Thomson, *Theoretical Aerodynamics*, Dover Publications Inc, New York, (1958).

[12] I. Proudman, J. Pearson, *Expansions at Small Reynolds Number for the Flow Past a Sphere and a Circular Cylinder*, J. Fluid Mech. 2, (1957), pp. 237-262.

[13] F. Sherman, *Viscous Flow*, McGraw-Hill series in Mechanical Engineering, New York, (1990).

[14] L. A. Skinner, *Generalized Expansions for Slow Flow Past a Cylinder*, Q. J. Mech. Appl. Math. 28, (1975), pp. 333-340.

[15] H. Takami, H. B. Keller, *Steady Two-Dimensional Viscous Flow of an Incompressible Fluid Past a Circular Cylinder*, Phys. Fluids Supp. II, (1969), pp. 51-56.

[16] D. J. Tritton, *Experiments on the Flow Past a Circular Cylinder at Low Reynolds Numbers*, J. Fluid Mech. 6, (1959), pp. 547-567.

[17] M. R. Trummer, *An Efficient Implementation of a Conformal Mapping Method Based on the Szegö Kernel*, SIAM J. Numer. Anal. 23, (1986), pp. 853-872.

[18] M. Van Dyke, *Perturbation Methods in Fluid Mechanics*, Parabolic Press, Stanford, (1975).

[19] M. J. Ward, W. Henshaw, J. B. Keller, *Summing Logarithmic Expansions for Singularly Perturbed Eigenvalue Problems,* SIAM J. Appl. Math. 53, (1993), pp. 799-828.

[20] M. J. Ward, S. A. Wolf, *On Perturbations of Cubic Fold Points for Nonlinear Eigenvalue Problems*, to appear, Methods and Applications in Analysis, (33 pages).

Appendix A: Analytical Results for the Generalized Model Problem

For our generalization (2.1) of Lagerstrom's model problem, the outer corrections u_j and the constants a_j are determined recursively from (2.3) and (2.7). From them we obtain the following formulae for the first few outer corrections:

$$\begin{aligned}
u_1(r) &= -E_1(r) \\
u_2(r) &= f^{'}(1)\left(2E_1(2r) - (1+e^{-r})E_1(r)\right) - \gamma E_1(r) \\
u_3(r) &= \left[f^{'}(1)\right]^2\left(-\frac{9}{2}E_1(3r) - \frac{3}{2}I(r) - \left(E_1(r) - 2e^{-r}\right)E_1(2r) + e^{-2r}E_1(r)\right) \\
&\quad + \left[f^{'}(1)\right]^2\left(\frac{e^{-r}}{2}(2-r)[E_1(r)]^2 - 2e^{-r}E_1(r) + 4E_1(2r)\right) \\
&\quad - 2\gamma f^{'}(1)\left(e^{-r}E_1(r) - 2E_1(2r)\right) + CE_1(r) \\
&\quad + f^{''}(1)\left(\frac{3}{2}I(r) + E_1(r)E_1(2r) - e^{-r}[E_1(r)]^2\right).
\end{aligned} \tag{A.1}$$

Here $E_1(r)$, $I(r)$ and C are defined by

$$\begin{aligned}
I(r) &\equiv \int_r^\infty e^{-\eta}[E_1(\eta)]^2\,d\eta\,, \qquad E_1(r) \equiv \int_r^\infty \frac{e^{-\eta}}{\eta}\,d\eta\,, \\
C &\equiv f^{''}(1)\log 2 - \frac{1}{2}\left[f^{'}(1)\right]^2(2\log 2 + 1) + 2\left(\log 2 - \gamma\right)f^{'}(1) - \gamma^2\,,
\end{aligned} \tag{A.2}$$

and γ is Euler's constant. The constants a_j, for $j \le 4$, defined in (2.7) and given in (2.9) are obtained from (A.1) by using the limiting behavior $E_1(r) = -\log r - \gamma + o(1)$ as $r \to 0$. In (2.9), the constant I is defined by $I \equiv I(0) \approx 1.22856$.

Appendix B: Some Analytical Results for Slow Viscous Flow

From [12], the solution to (3.7a), which satisfies $\Psi_1 \sim \rho\log\rho\sin\theta$ as $\rho\to 0$ is

$$\Psi_1(\rho,\theta) = -\sum_{n=1}^{\infty}\frac{c_n(\rho/2)}{n}\rho\,\sin(n\theta)\,, \qquad c_n(s)\equiv 2\left[K_1(s)I_n(s)+K_0(s)I_n^{'}(s)\right]\,. \tag{B.1}$$

As $\rho\to 0$, $c_n(\rho/2)=O(\rho^{n-1})$ for $n>1$, and $c_1(\rho/2)\sim 1-\log(\rho/4)-\gamma$, where γ is Euler's constant. Thus, $\Psi_1-\rho\log\rho\sin\theta\to\rho\big(\gamma-\log 4-1\big)\sin\theta$ as $\rho\to 0$, and hence, from (3.7b), $a_2=\gamma-\log 4-1$.

To evaluate numerically the Jacobian in the hybrid formulation (4.11), we use the following analytical formulae for various derivatives of $\Psi_1(\rho,\theta)$:

$$\begin{aligned}
2\,\partial_\rho\nabla^2\Psi_1 &= e^{x/2}\,\sin\theta\,\left[K_1(\rho/2)\cos\theta-K_0(\rho/2)-2\rho^{-1}K_1(\rho/2)\right]\,,\\
2\,\partial_\theta\nabla^2\Psi_1 &= e^{x/2}K_1(\rho/2)\,\left[2\cos\theta-\rho\sin^2\theta\right]\,,\\
\partial_\rho\Psi_1 &= -e^{x/2}K_0(\rho/2)\sin\theta\,,\\
\partial_\theta\Psi_1 &= -\rho\,e^{x/2}\left[K_1(\rho/2)+K_0(\rho/2)\cos\theta\right]+2\,.
\end{aligned} \tag{B.2}$$

Here $x=\rho\cos\theta$. In terms of x and $y=\rho\sin\theta$, the Oseen vorticity, denoted by $-\omega_1$, and the components of the Oseen velocity are given by (see [8])

$$\begin{aligned}
u_1 &= \partial_y\Psi_1 = -2\,e^{x/2}K_0(\rho/2)+2\,\partial_x\left[e^{x/2}K_0(\rho/2)+\log\rho\right]\,,\\
v_1 &= -\partial_x\Psi_1 = 2\,\partial_y\left[e^{x/2}K_0(\rho/2)+\log\rho\right]\,,\\
\omega_1 &= \nabla^2\Psi_1 = -y\rho^{-1}\,e^{x/2}K_1(\rho/2)\,.
\end{aligned} \tag{B.3}$$

Kaplun's method (see [5]) to determine a_3 in (3.8b) is to first decompose Ψ_2 as $\Psi_2=a_2\Psi_1+\Psi_{2p}$ and then introduce $\mathbf{u}_{2p}$ by $\mathbf{u}_{2p}=\big(\partial_y\Psi_{2p},-\partial_x\Psi_{2p}\big)$. It then follows from (3.8a) that

$$\begin{aligned}
\big(\nabla^2-\partial_x\big)\,\mathbf{u}_{2p} &= -\nabla P_2+\mathbf{F}(x,y)\,,\\
\nabla\cdot\mathbf{u}_{2p}=0\,, &\qquad \mathbf{F}\equiv\big(F_1,F_2\big)=\omega_1\big(v_1,-u_1\big)\,,
\end{aligned} \tag{B.4}$$

where P_2 is an unknown pressure. The solution to (B.4) can be represented in terms of the Green's matrix of the homogeneous operator. From this representation, and by using the condition from (3.8b) that $\mathbf{u}_{2p}\to(a_3-a_2^2)\mathbf{i}$ as $\rho\to 0$, one can obtain the following equation for a_3:

$$a_3 = a_2^2-\frac{1}{2\pi}\int_{-\infty}^{\infty}\int_{-\infty}^{\infty}\left[g_{11}(-x,-y)F_1(x,y)+g_{12}(-x,-y)F_2(x,y)\right]\,dx\,dy\,. \tag{B.5a}$$

Here g_{11} and g_{12}, which are elements of the Green's matrix, are defined by

$$g_{11}(x,y) = -e^{x/2}K_0(\rho/2)+\partial_x\left[e^{x/2}K_0(\rho/2)+\log\rho\right]\,,\quad g_{12}(x,y)=\partial_y\left[e^{x/2}K_0(\rho/2)+\log\rho\right]\,. \tag{B.5b}$$

From (B.3), (B.4) and (B.5b), a lengthy calculation shows that (B.5a) can be expressed in terms of polar coordinates as

$$a_3 = a_2^2-\frac{1}{2\pi}\int_0^{\infty}\int_0^{2\pi}K_0(\rho/2)K_1(\rho/2)\left[1+e^{\rho\cos\theta}-\rho\,e^{(\rho/2)\,\cos\theta}K_1(\rho/2)\right]\,\sin^2\theta\,d\theta\,d\rho\,. \tag{B.6}$$

Finally, the result (3.9) for a_3 follows from (B.6) by using the identity $\int_0^{2\pi} e^{\rho\cos\theta}\sin^2\theta\,d\theta = 2\pi\rho^{-1}I_1(\rho)$. We obtained the numerical value for the integral in (3.9) from a careful numerical quadrature.

A formula for the drag coefficient C_D is given in [4] in terms of an arbitrary closed contour around the body. From this formula and from the symmetry of the flow, it follows that

$$\begin{aligned} C_D = r\int_0^\pi \left[\cos\theta\big(\psi_r^2 - \frac{1}{r^2}\psi_\theta^2\big) - \frac{2}{r}\sin\theta\,\psi_r\psi_\theta\right]\,d\theta - 2r\int_0^\pi \omega\,\psi_\theta\sin\theta\,d\theta \\ - 2\epsilon^{-1}r\int_0^\pi (r\omega_r - \omega)\,\sin\theta\,d\theta\,, \end{aligned} \tag{B.7}$$

where ψ satisfies (3.1) and $\omega = \nabla^2\psi$. Here r is the radius of an arbitrary circular contour that encloses the body. The result (3.10a), which holds for $\epsilon \to 0$ and for an arbitrarily shaped body, is obtained by evaluating (B.7) on a large circle (i. e. $r = r_0 \gg 1$), where the far field form (3.5b) for the Stokes expansion can be used. For a circular cylinder of radius one, we can evaluate (B.7) conveniently on $r = 1$ to obtain the exact formula

$$C_D = 2\epsilon^{-1}\int_0^\pi (\omega - \omega_r)\,\sin\theta\,d\theta\,. \tag{B.8}$$

ϵ	$Q(\epsilon)$	$Q^*(\epsilon d)$	(4 term)	(3 term)	(2 term)
0.0104	0.1889	0.1892	0.1888	0.1923	0.1984
0.0517	0.2608	0.2620	0.2590	0.2722	0.2891
0.1089	0.3126	0.3140	0.3045	0.3349	0.3665
0.2409	0.3884	0.3868	0.3422	0.4369	0.5109
0.3399	0.4296	0.4232	0.3225	0.4974	0.6146
0.4759	0.4753	0.4596	0.2107	0.5649	0.7640
0.6430	0.5204	0.4908	-0.1364	0.6199	0.9715
0.7574	0.5465	0.5064	-0.5934	0.6314	0.1136
0.9703	0.5877	0.5272	-2.3490	0.5513	0.1515

Table 1: For $\kappa = 1$ $(d = e^{-1})$ and $f(u) = u,$ the hybrid result $Q^*(\epsilon d)$ is compared with the exact result $Q(\epsilon)$ and with the truncated series (2.8), (2.9) .

δ	θ_T	k	c	d	b
.050	0°	2.000	0.961	0.328	0.040
.080	5°	1.972	0.952	0.344	0.066
.100	13°	1.928	0.960	0.354	0.082
.120	16°	1.910	0.954	0.364	0.098
.120	20°	1.889	0.968	0.363	0.096
.200	25°	1.861	0.915	0.410	0.170

Table 2: Numerical values for d corresponding to the Karman Trefftz airfoils (4.7). The tail angle (in degrees) is θ_T and the thickness ratio is δ . The last column gives the value of b for an ellipse, with $a = 1,$ that has the same value of d as the corresponding airfoil.

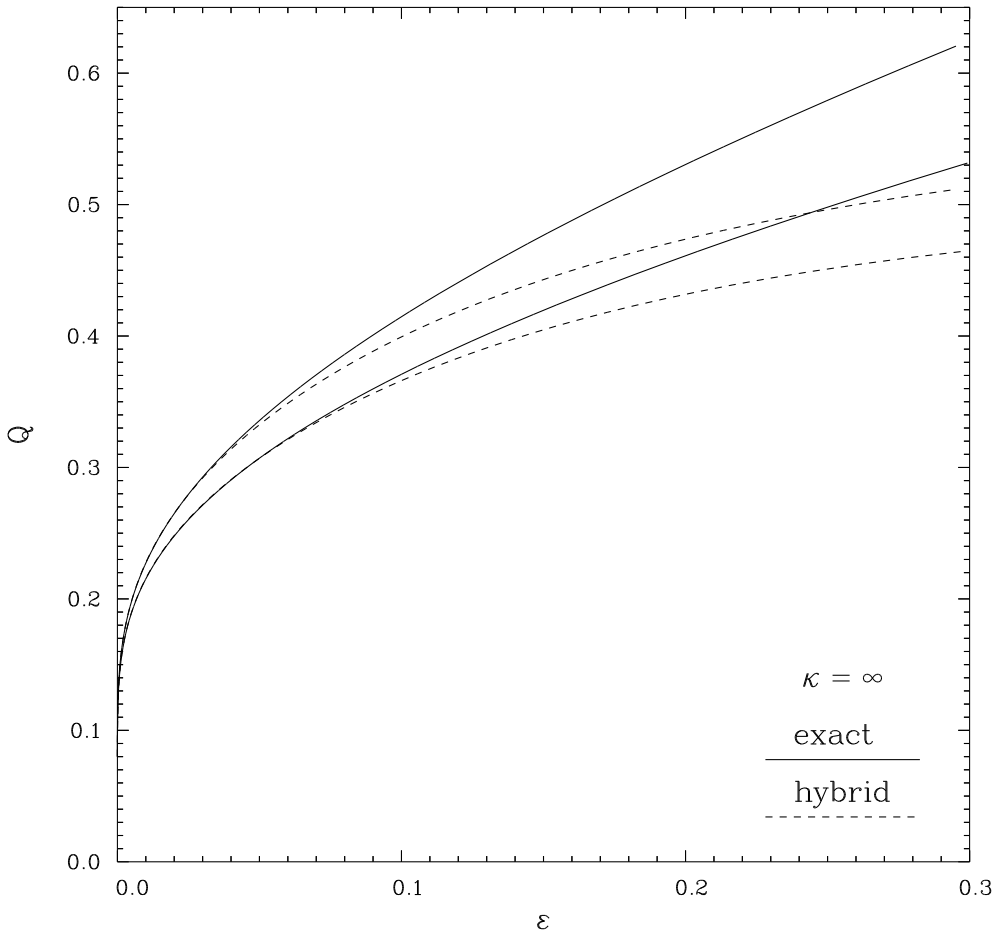

Fig. 1: For $\kappa = \infty$ ($d = 1$) and for two forms of $f(u)$, $Q^*(\epsilon)$ is compared with the full numerical result for $Q(\epsilon)$. The top two curves are for $f(u) = u$ and the bottom two curves are for $f(u) = 2u^3/(1+u^2)$.

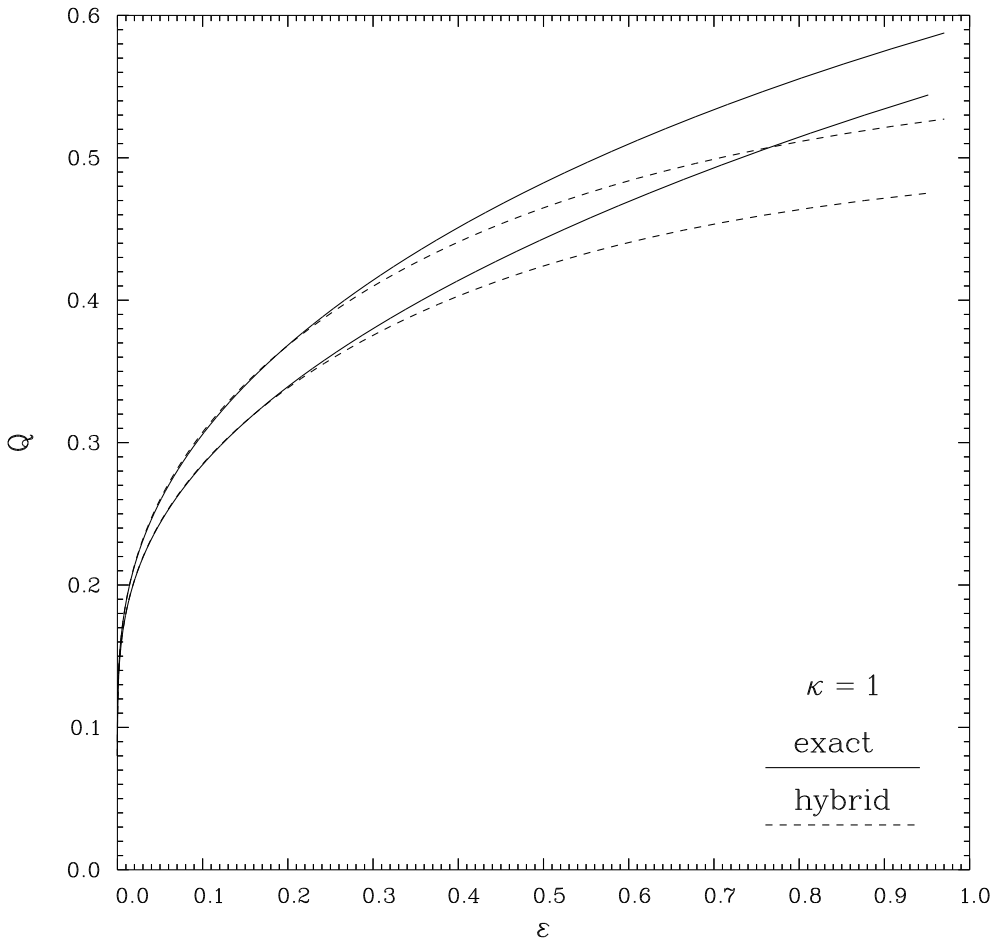

Fig. 2: Same caption as for Fig. 1 except that the results are now compared at $\kappa = 1$ ($d = e^{-1}$).

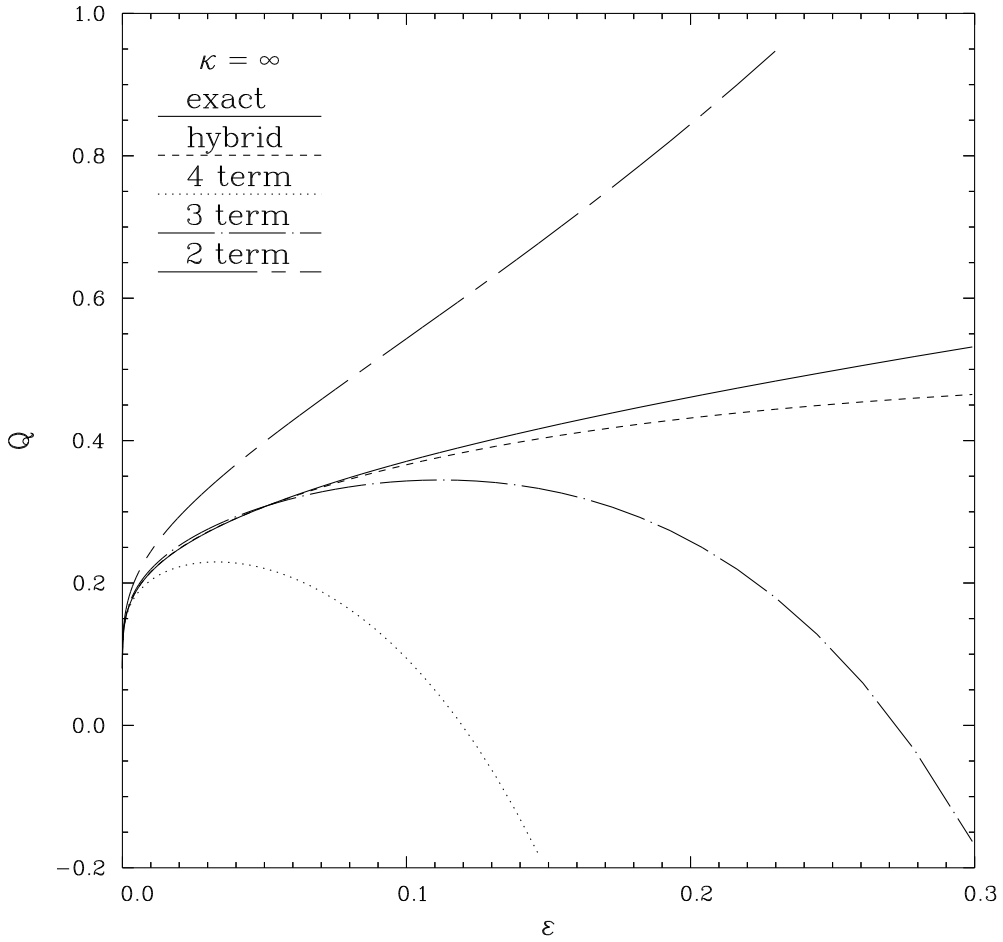

Fig. 3: For $\kappa = \infty$ and $f(u) = 2u^3/(1+u^2)$, the hybrid result $Q^*(\epsilon)$ is compared with the exact result and with the two, three, and four term expansions obtained from (2.8) and (2.9).

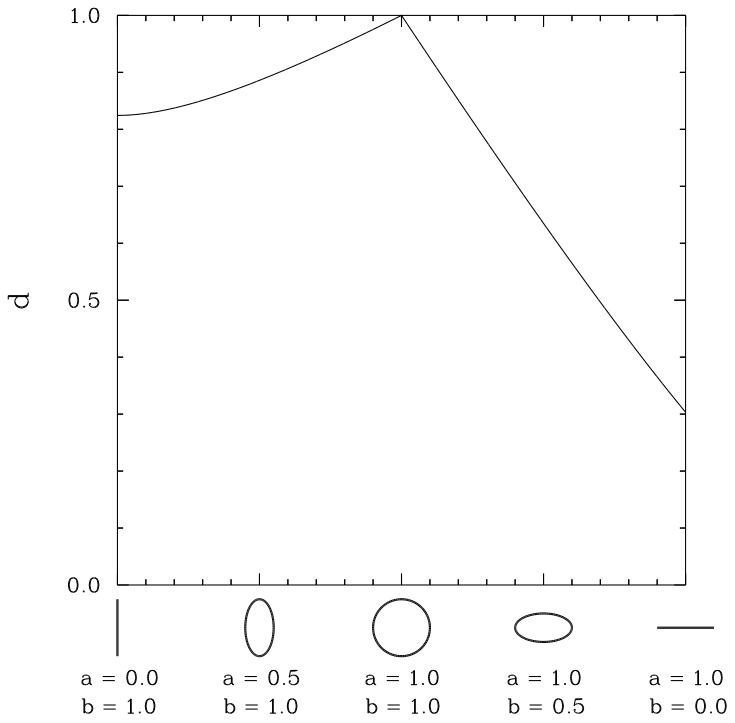

Fig. 4: Plot of d, obtained from (3.19), for an ellipse where the semi-major axis is 1.

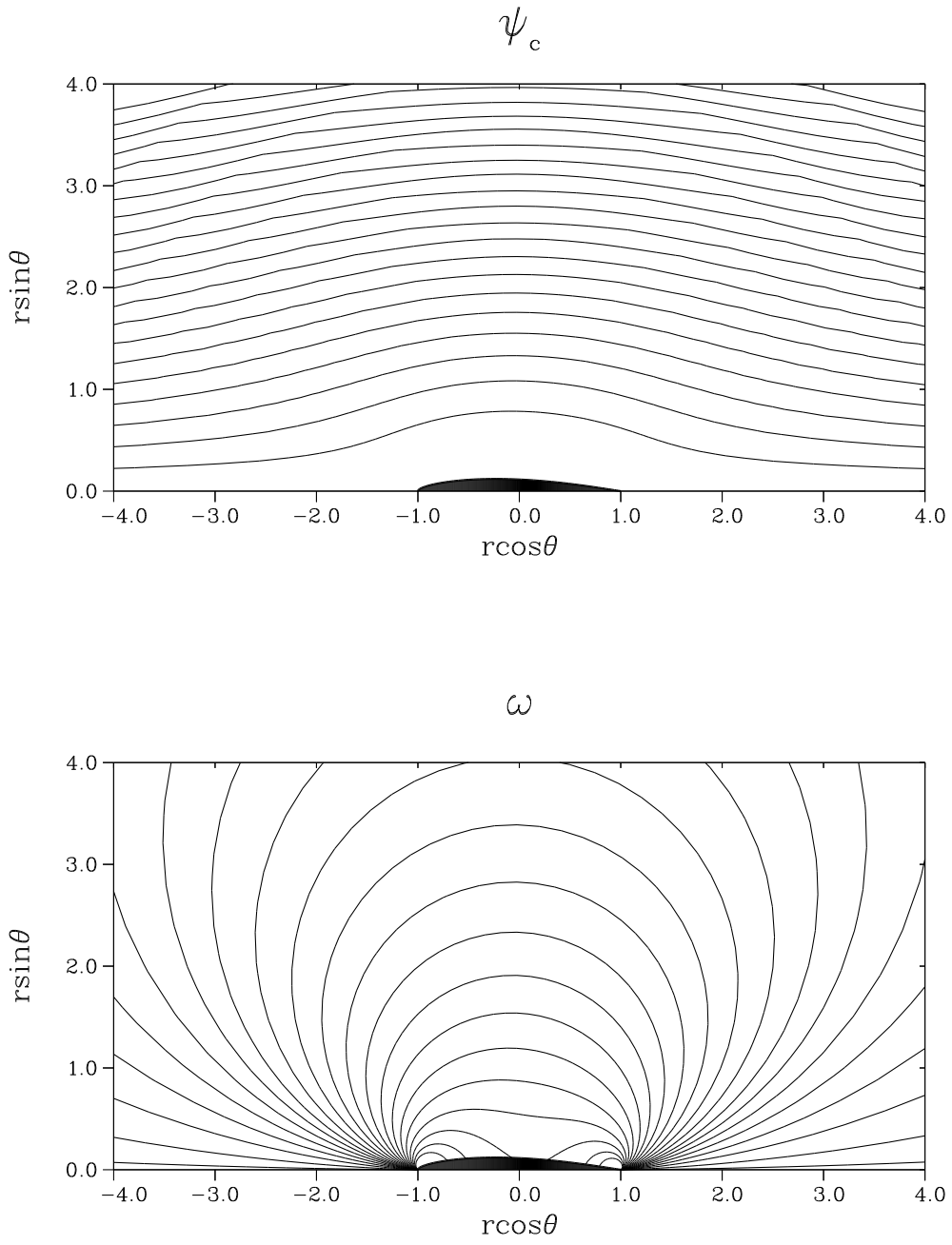

Fig. 5: Contour plots of the stream function and the vorticity, computed from (4.5), for Stokes flow around the Karman-Trefftz airfoil (4.7) with $\kappa = 1.91$ and $c = 0.954$.

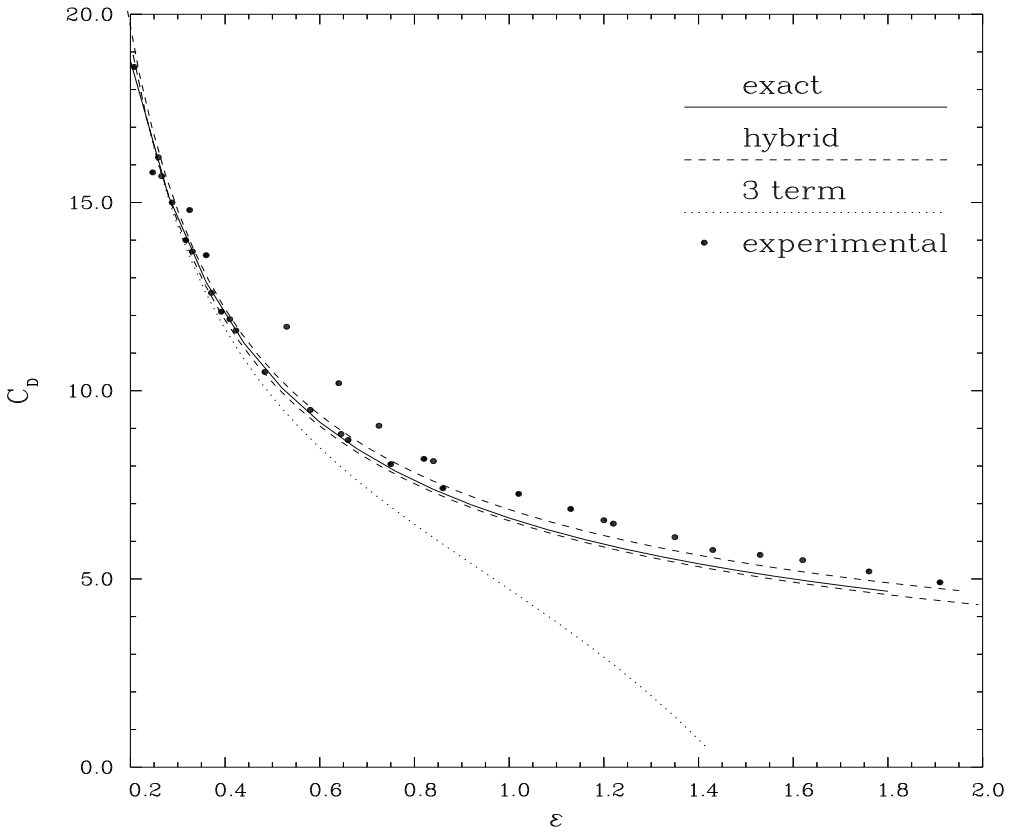

Fig. 6: For a circular cylinder, the hybrid results for C_D versus the Reynolds number ϵ are compared with experimental results, with the three-term expansion (3.10b), and with the full numerical results. The top hybrid curve corresponds to A^*_{max} and the bottom curve corresponds to A^*_{min}.

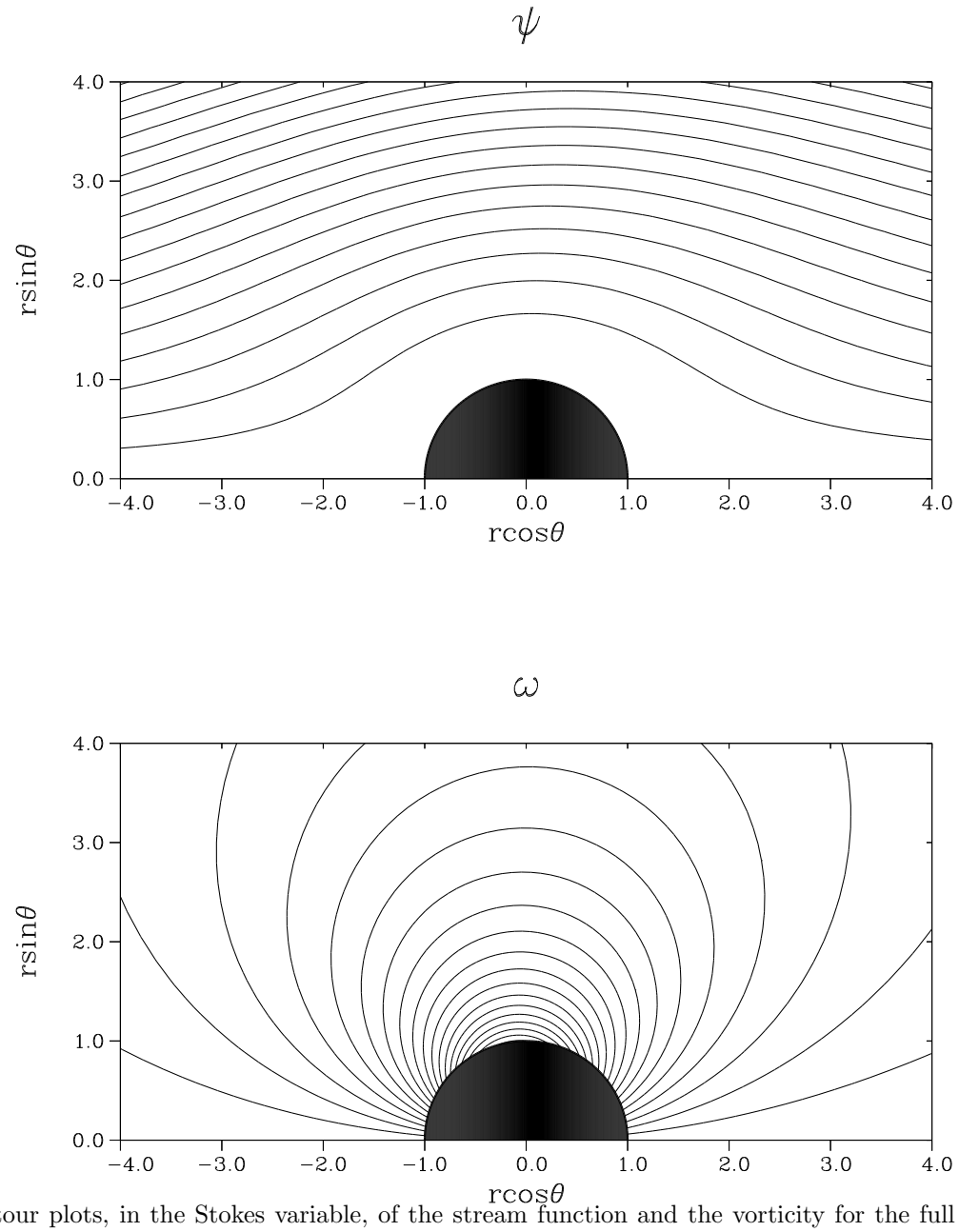

Fig. 7: Contour plots, in the Stokes variable, of the stream function and the vorticity for the full flow over a circular cylinder computed from (4.13) with $\epsilon = 0.085$. Notice that the full flow field has a very slight upstream/downstream asymmetry.

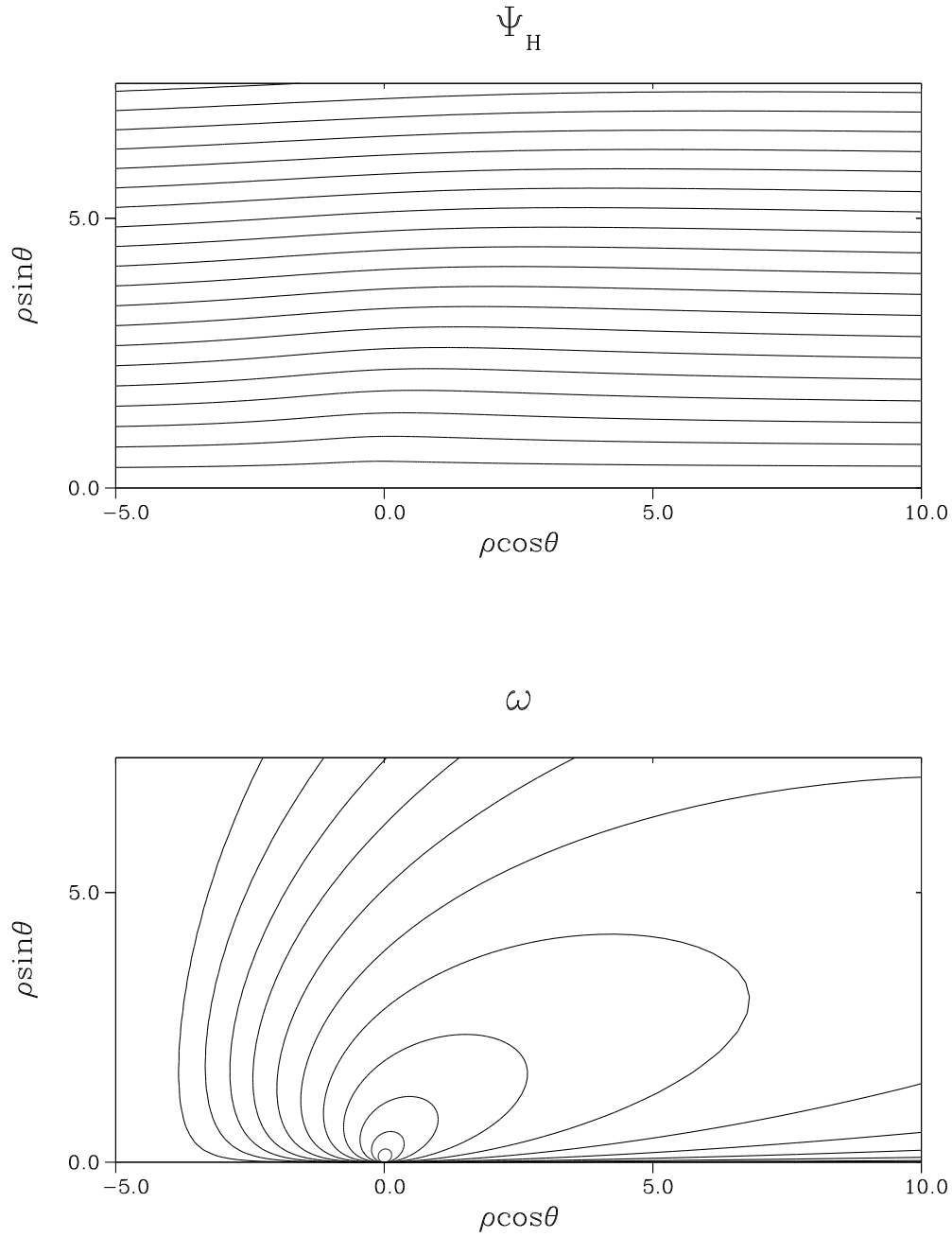

Fig. 8: Contour plots, in the Oseen variable, of the stream function and the vorticity computed from the hybrid problem (4.10) with $\kappa = 0.25$ ($\epsilon \approx 0.085$).

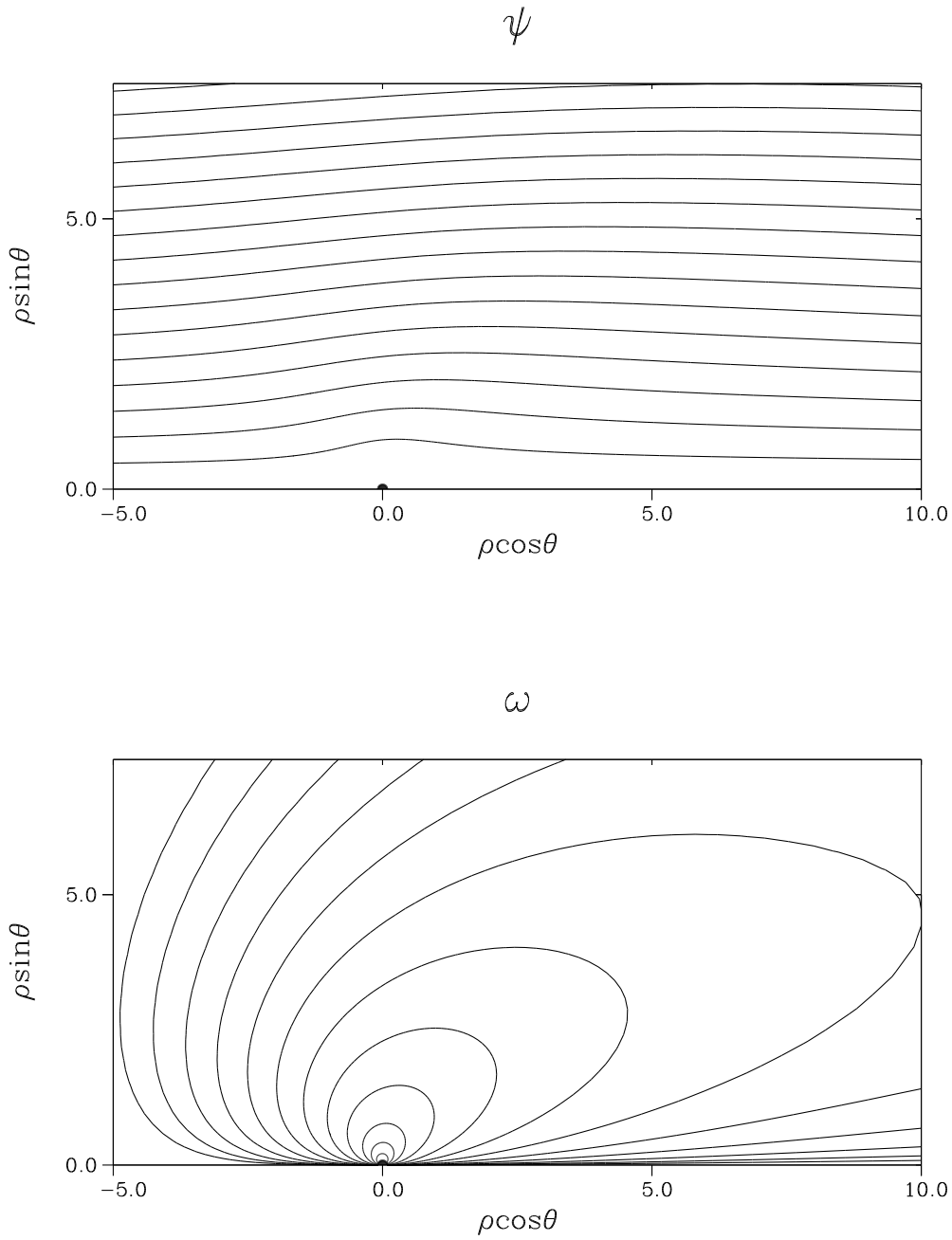

Fig. 9: Contour plots, in the Oseen variable, of the stream function and the vorticity computed from the full problem (4.13) with $\epsilon = 0.085$.

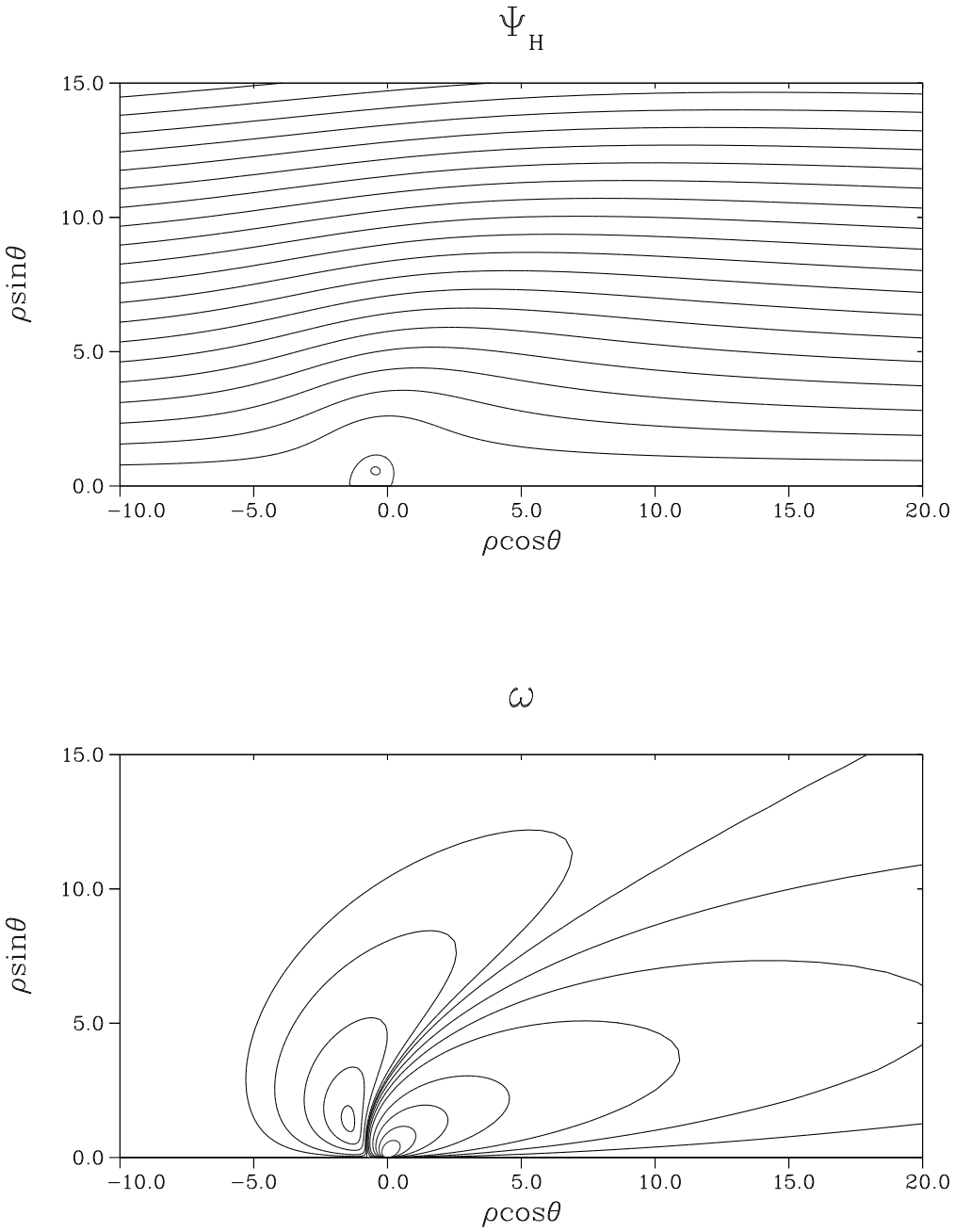

Fig. 10: Contour plots, in the Oseen variable, of the stream function and the vorticity computed from the hybrid problem (4.10) with $\kappa = 0.65$ ($\epsilon \approx 1.65$).

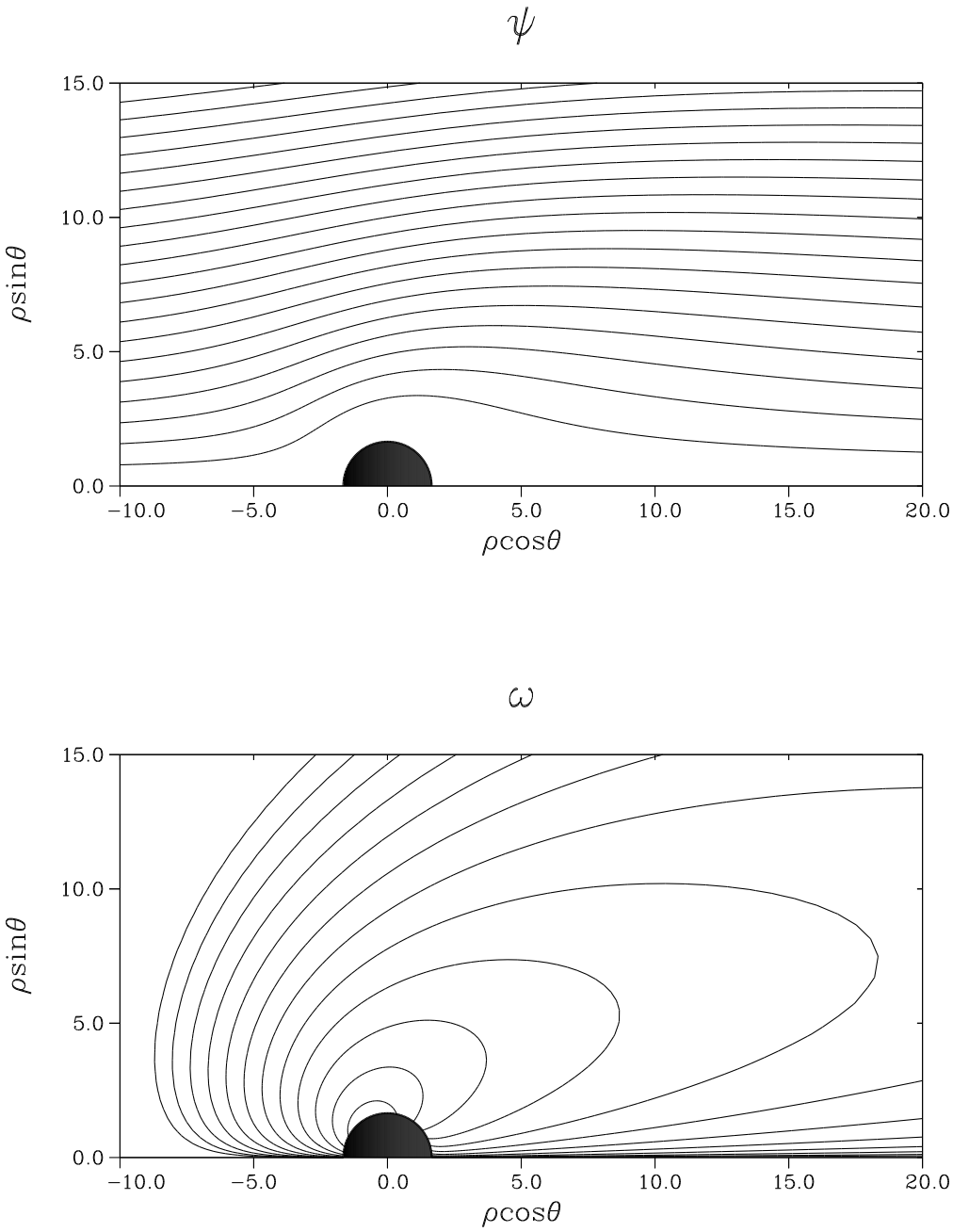

Fig. 11: Contour plots, in the Oseen variable, of the stream function and the vorticity computed from the full problem (4.13) with $\epsilon = 1.65$.

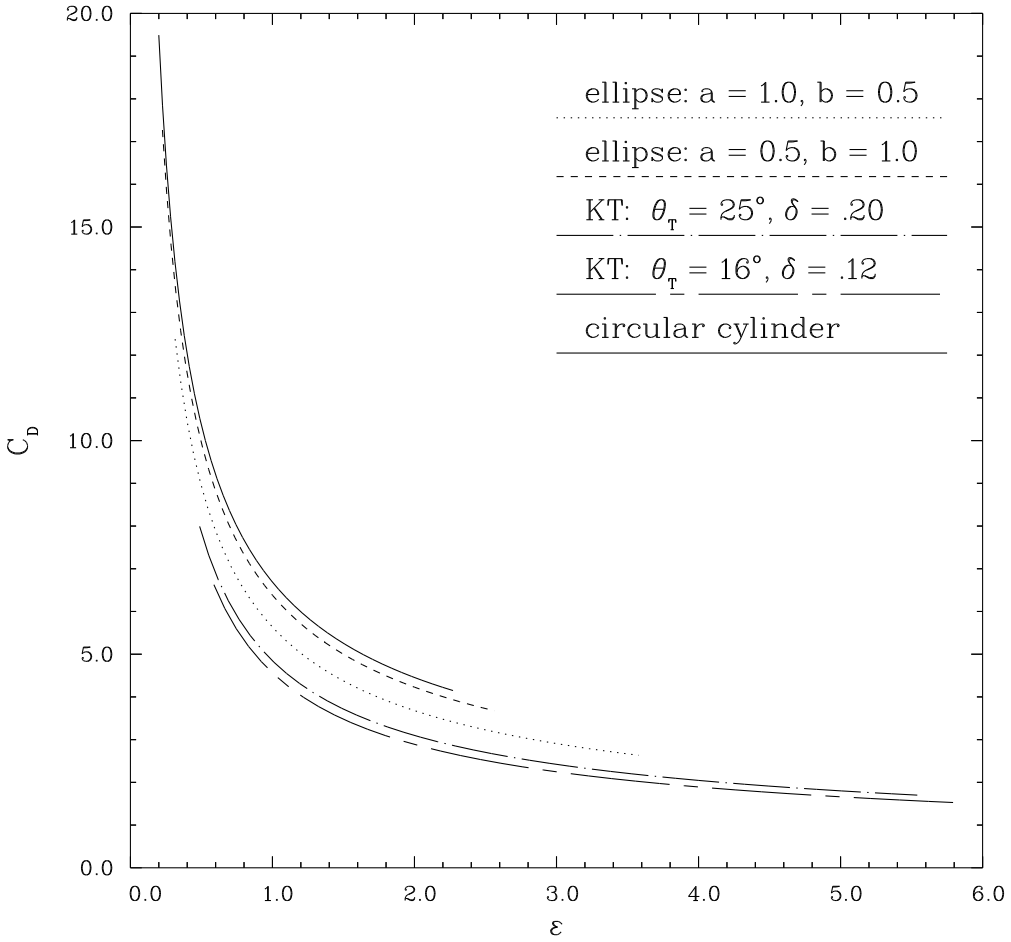

Fig. 12: Plots of the hybrid drag coefficient for cylinders of various cross-sectional shapes.

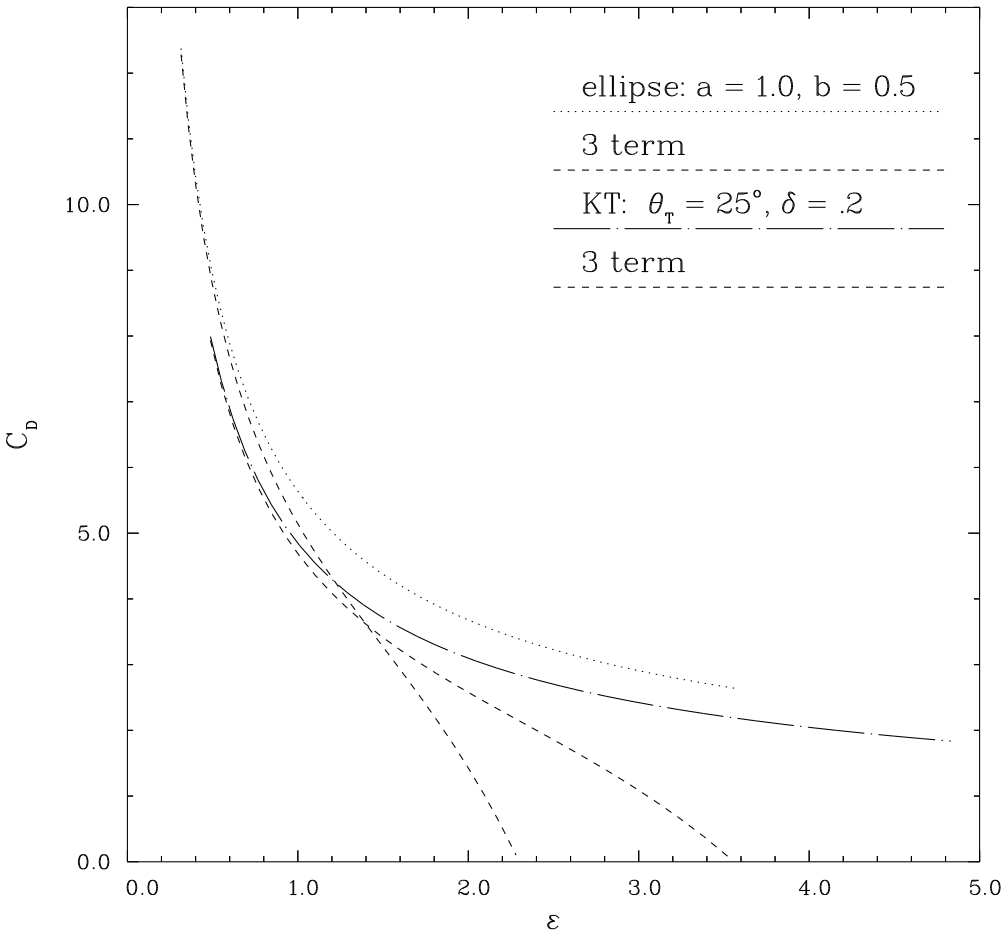

Fig. 13: The hybrid drag coefficient is compared with the three-term result (3.10*b*) for a cylindrical body with either an elliptical or a Karman-Trefftz airfoil cross-section.